TEKNILLINEN KORKEAKOULU
Faculty of Electronics, Communications and Automation
Department of Automation and Systems Technology

Mirva Jääskeläinen

Experimental Study on Droplet Self-alignment Assisted Robotic Microhandling

Master's thesis submitted in partial fulfilment of the requirements for the degree of Master of Science in Technology

Espoo, 1st Dec 2009

Supervisor, Instructor: Docent Quan Zhou, Doctor of Science (Technology)

HELSINKI UNIVERSITY OF TECHNOLOGY Faculty of Electronics, Communications and Automation Department of Automation and Systems Technology	ABSTRACT OF MASTER'S THESIS

Author	Mirva Jääskeläinen	Date	1st Dec 2009
		Pages	6 + 85
Title of thesis	Experimental Study on Droplet Self-alignment Assisted Robotic Microhandling		
Professorship	Control Engineering	Code	AS-74
Supervisor, Instructor	Docent Quan Zhou, Doctor of Science (Technology)		

The main objective of this thesis is to experimentally study the effect of different process parameters on the results of a hybrid microassembly method previously developed at TKK. The hybrid method is a combination of robotic microhandling and droplet self-alignment.

The survey part of the thesis has two sections. The first part gives an overview of the microworld and the state-of-the-art of microassembly methods including both robotic and self-assembly methods. The second part concentrates on capillary force and its applications in microhandling.

The experimental method, the test set-up and key test parameters are discussed in the second part of the thesis. The key parameters include biases (the initial error in the part location before self-alignment) in three axes, the amount of liquid for self-alignment and the size of the parts. Moreover, the test procedure is described in details.

Several sets of tests were conducted and the results are analyzed carefully in the third, experimental part of the thesis. Especially the success rates and areas of success as a function of different parameters are studied and compared. The accuracy of the final assembly is analyzed by a scanning electron microscope.

The results show that the hybrid microassembly method is reliable for assembling microparts. The study on the effects of the process parameters prove that accuracy requirements of the handling robot are very low while the accuracy obtained with the method is in the range of 1-2 μm, comparable with what has been achieved by self-assembly.

Keywords: Microassembly, hybrid handling, droplet self-alignment

TEKNILLINEN KORKEAKOULU Elektroniikan, tietoliikenteen ja automaation tiedekunta Automaatio- ja systeemitekniikan laitos		DIPLOMITYÖN TIIVISTELMÄ
Tekijä	Mirva Jääskeläinen	Päiväys: 1. joulukuuta 2009 Sivumäärä: 6 + 85
Työn nimi	Kokeellinen tutkimus robotiikaa ja pisaran itseasennoitumista hyödyntävästä mikrokokoonpanosta	
Professuuri	Systeemitekniikka	Koodi: AS-74
Valvoja, ohjaaja	Dosentti Quan Zhou, Tekniikan tohtori	

Tämän diplomityön päätavoite on tutkia kokeellisesti eri prosessiparametrien vaikutusta Teknillisessä korkeakoulussa kehitetyn hybridimenetelmän tuloksiin mikrokokoonpanossa. Menetelmässä yhdistetään robottimikrotarttujan käyttö ja mikrokappaleiden pisara-avusteinen itseorganisoituminen kapillaarivoimien avulla.

Työn selvitysosuudessa on kaksi osiota. Ensimmäisessä osiossa tutustutaan mikrokokoluokan erityispiirteisiin ja mikrokokoonpanomenetelmiin sekä robottiavusteisten ja itseorganisoituvuutta käyttävien menetelmien kautta. Toisessa osiossa keskitytään kapillaarivoimaan ja sen sovelluksiin mikrokappaleiden käsittelyssä.

Kokeellinen menetelmä ja koelaitteisto esitellään työn toisessa osuudessa. Myös parametrit, joita ovat vapautuspaikan ero lopulliseen paikkaan, nesteen määrä ja palan koko, esitellään tarkemmin. Testien kulun yksityskohdat käsitellään.

Kokeellisessa osassa suoritettujen testien tulokset esitetään. Kokoonpanon onnistumistodennäköisyyttä tarkastellaan ja vertaillaan eri prosessiparametrien funktiona. Menetelmän tarkkuutta arvioidaan pyyhkäisyelektronimikroskooppikuvien avulla.

Tulokset osoittavat, että tutkitulla robotiikaa ja pisaran itseasennoitumista hyödyntävällä menetelmällä voidaan luotettavasti kokoonpanna mikrokappaleita. Saavutettu tarkkuus (1-2 μm) on vertailukelpoinen itseorganisoitumista käyttävien menetelmien kanssa.

Avainsanat: Mikrokokoonpano, hybridimenetelmä, itseorganisoituminen

Preface

This thesis has been made in the Department of Automation and Systems Technology, Faculty of Electronics, Communications and Automation, at Helsinki University of Technology. This work has been supported by the European Commission under the grant NMPZ-CT-2006-026622 Hybrid ultra precision manufacturing process based on positional- and self-assembly for complex micro-products, HYDROMEL (2006-2010).

I wish to express my deepest gratitude to my supervisor and instructor, doctor Quan Zhou, who guided me and has made a great effort in commenting on this work extensively. I thank Veikko Sariola who helped me with patience during the experimental part of this thesis and gave me valuable comments during the writing process. Moreover, I would like to thank Veikko Sariola and Bo Chang for the contribution to the accuracy analysis of the test results. The whole Control Engineering research group and especially all the members of the Micro- and Nanorobotics team in the Department of Automation and Systems Technology have established a comfortable working atmosphere. Moreover, I'm grateful for William Martin who proofread the thesis.

Finally, I would like to thank my husband, who has tolerated my long working hours and has supported me all the time, and my parents for their encouragement during the course of my studies.

Espoo, December 2009

Mirva Jääskeläinen
Rummunlyöjänkatu 3 A 2
FIN-02600 Espoo
tel. +358 40 046 4828

Contents

Symbols and Abbreviations

Roman letters

F_C	Capillary force
F_g	Gravitational force
F_L	Laplace force
F_T	Tension force
g	Gravitational acceleration
H	Mean surface curvature
L	Typical linear dimension
m	Mass of an object
P_{int}	Pressure on the internal side of the surface
P_{out}	Pressure on the external side of the surface
r	Contact circle radius
V	Volume of an object
W	Surface energy
z	Separation distance

Greek letters

γ	Surface tension
γ_{LV}	Surface tension on liquid-vapor interface
γ_{SL}	Surface tension on solid-liquid interface
γ_{SV}	Surface tension on solid-vapor interface
θ	Contact angle
ρ	Density

Abbreviations

DC	Direct Current
CCD	Charge-Coupled Device
DOF	Degree of Freedom
LED	Light-Emitting Diode
MA	Mean Absolute
MEMS	Micro-Electro Mechanical Systems
NEXUS	The Network of Excellence in Multifunctional Microsystems
PZT	Lead Zirconate Titanate
RFID	Radio Frequency Identification
RMS	Root Mean Square
SA	Self-assembly
SAM	Self-assembled Monolayer
SEM	Scanning Electron Microscope
semi-DUO-SPASS	Semidry uniquely orienting process
SU-8	Epoxy-based negative photoresist
TKK	Helsinki University of Technology

Chapter 1

Introduction

Microsystem technology is a wide discipline of manufacturing mechatronics, electronics, optics and fluidics in microscale. Microengineered devices are often heterogenous – composed of components made by different manufacturing processes and assembled finally into a system. The miniaturization of the components makes the assembly difficult. There often is also a significant difference in size between the components which complicates the assembly task.

Handling and assembly of those devices is challenging because the magnitudes of the forces are different in microscale than in macroscale. Adhesion forces become dominant and cause problems such as the manipulated object sticking to the gripper. Moreover, observation of the process is difficult because the depth of field is small, and a bright and even illumination must be produced in multiple axes.

Robotic microhandling typically uses components such as a microgripper, a positioning system, sensors and a control system. The accuracy of robotic microhandling methods depends on the accuracy of the sensors and microscopes used. Another approach proposed to handle microscopic object is self-assembly: the accuracy requirements can be fulfilled without accurate sensors and also adhesion problems can be overcome when no gripper is needed. In self-assembly the principle of minimal potential energy drives the

system autonomously towards order. Hybrid assembly is a new approach to microhandling combining the good characteristics of both branches.

The objective of this thesis is to study the possibilities of the hybrid microhandling technique developed at TKK. The technique combines tweezers and self-assembly by dispensing water droplets to help the handled part to detach from the gripper tips and let the part to self-align to the desired position. The handling is done with SU-8 microparts.

Fig. 1.1 shows a typical hybrid microhandling sequence. An assembly site is on a working surface (a), and a droplet of water is dispensed on it (b). A microgripper carries the part to the releasing position and descends (c). When the droplet contacts with the top part a meniscus is formed (d). The microgripper releases the part (e). Capillary force aligns the parts and the water evaporates (f).

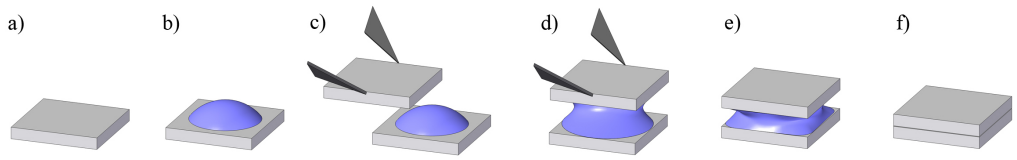

Figure 1.1: Hybrid handling method.

Different process parameters affect the results of the hybrid handling, for example, the bias (which means the initial error in the part location before self-alignment), the amount of liquid, size of the parts and shape of the parts. The effect of these parameters is studied in this thesis.

Chapter 2 reviews the literature on the current state-of-the-art of different microassembly techniques. Robotic assembly and self-assembly are discussed and the concept of hybrid assembly is presented. The chapter also discusses the basic physical principles behind the main problems in the microhandling.

The physical phenomena behind the capillary self-alignment, applications and previous studies of the subject are discussed in Chapter 3.

Chapter 4 introduces the experimental design. The objectives and the parameters of the study are discussed and the experimental set-up and the test procedure are presented.

Chapter 5 discusses the experimental results. The effects of different parameters in the assembly of microparts of the same and different sizes are analyzed and the results are compared. Chapter 6 concludes the thesis.

Chapter 2

Microhandling and Microassembly

2.1 Microhandling and -assembly concepts

Robotic microhandling has been actively studied since the late 80s and the early 90s (Hunter et al., 1989; Fukuda and Tanaka, 1990). Microhandling stands for a group of techniques for operating microscopic objects, which have dimensions smaller than 1mm. Those techniques include, for example, picking, placing, positioning, assembly, cutting, micromilling, indentation, aspiration and different microinjection techniques. Also, the term micromanipulation has been used.

The main application areas for microhandling are bio- and medical technology and microsystems. In microsystems, microhandling is needed in the assembly of for example RFID tags, micromotors and accelerometers. The bio- and medical technology branch has applications like, for instance, biochips, bioMEMS (Micro-Electro-Mechanical Systems), Lab-On-Chips, micro implants and drug delivery systems. Moreover, minimal-invasive surgery is one of the research fields of medical technology (more examples are found in Fig. 2.1.)

In Fig. 2.1 the market distribution of the most popular microsystem technology and MEMS products is presented. The analysis was made in 2006 by NEXUS (The Network of Excellence in Multifunctional Microsystems) and it reveals that read-write heads, inkjet heads and MEMS displays make up the most of the market (Salomon, 2006). Microhandling plays an important role in the manufacturing processes of these microsystems.

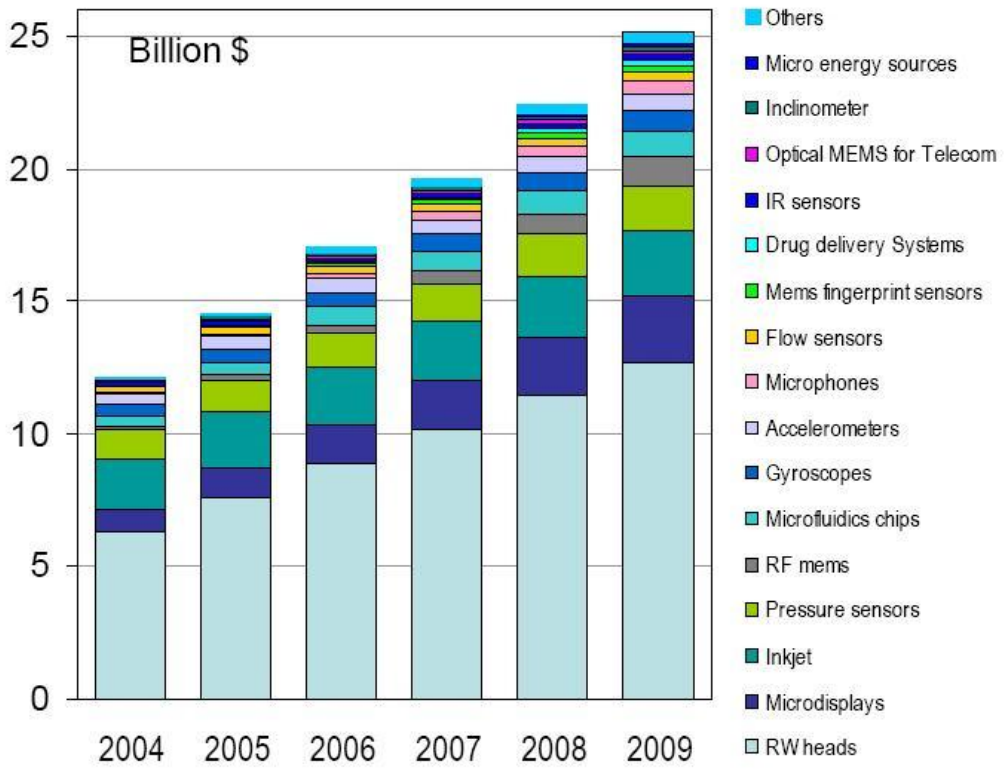

Figure 2.1: Division of the markets of microsystem/MEMS products according to NEXUS. Reprinted from Salomon (2006) with permission.

Microassembly refers to the assembly of microscopic objects. Microhandling in that context is used to manipulate the objects in a way that they will go to the desired place and will stay there either temporarily or permanently. The typical accuracy has a range of 0.1-10.0 µm (Tichem et al., 2004). In this section the different microhandling techniques are introduced in the context of microassembly.

2.2 Microworld

There is no general definition for the size of a microcomponent. Components having dimensions varying from micrometer range to a few centimeters are sometimes called microcomponents. In this thesis, however, the term microscale stands for the range smaller than 1 mm. To get an idea of the scale, one can think about a human hair fibre, which has a thickness of 50-100 µm.

2.2.1 Scaling effect

The reason why conventional handling techniques cannot be applied to microscopic objects is the scaling effect. The term stands for the change in the dominant physical quantities between different scales (see Table 2.1).

Table 2.1: Predominant forces, adapted from Lambert and Régnier (2006).

Interaction distance	Predominant force
Up to infinite range	Gravity
From a few nm up to 1 mm	Capillary forces
from 0.3 nm	Electrostatic forces
from 0.3 nm up to 100 nm	van der Waals
less than 0.3 nm	Molecular interactions
0.1 - 0.2 nm	Chemical interactions

Scaling laws tell how different quantities depend on L, the typical linear dimension (distance or length). Since area is proportional to L^2, its scaling law is L^2. In the same way volume has a scaling law of L^3. Forces scale as well. For example, gravitational force $F_g = mg$ scales as volume, L^3, since $m = \rho V$ and g is the gravitational acceleration, which is constant. However, the adhesion forces, for example, van der Waals force, vary as the contact area, L^2. Since gravity and van der Waals force vary differently depending on L, the magnitude of their effect is dependent on the size. There is a limit when adhesion forces become more effective than gravity when the size is decreased – that is why gravitation can often be neglected in the microworld (Trimmer, 1989; Shimoyama, 1995; Wautelet, 2001).

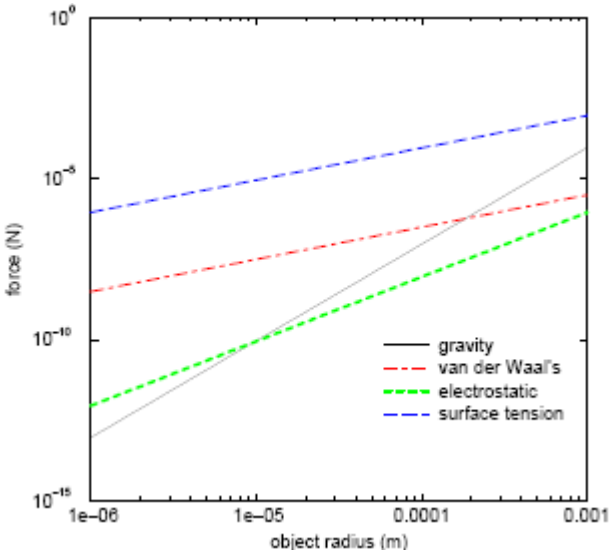

Figure 2.2: Gravitational, electric, van der Waals and surface tension forces. Attractive forces between sphere and plane (Fearing, 1995). Copyright ©1995 IEEE.

As scaling laws show us, in small scale the gravitational and inertial forces become less effective while adhesion forces become more important. The change in the scales of the forces can be seen in Fig. 2.2. Adhesion forces (van der Waals, capillary and electrostatic forces) may cause problems in gripping procedure. In macroscale the gravitational forces dominate the handling process and the handled object will drop when a gripper opens. In microscale the adhesion forces dominate and the gravitational forces become insignificant which may prevent the release of the part.

Also, friction has to be considered differently in microscale. In macroscale it is independent of the contact area, but in microscale the area has to be taken into consideration – that is caused by surface roughness. The combination of friction and adhesion forces is called striction (Wautelet, 2001).

2.2.2 Adhesion forces

The term van der Waals forces refers to the attractive or repulsive forces between molecular entities or inside them. Definitions vary and sometimes the term refers only to attractive forces. There are three types of interactions:

dipole-dipole, dipole-induced dipole and London (instantaneous induced dipole-induced dipole) forces (Israelachvili, 1985; IUPAC, 1997). Van der Waals forces have a very short effective distance (see Table 2.1). That is why they are not so significant in microhandling where distance is usually larger than that due to surface roughness (Fearing, 1995).

Electrostatic forces are due to electrostatic charges, which either repel or attract each other. They can be also due to contact electrification (Israelachvili, 1985). Fearing (1995) argues in his study that electrostatic force is the most significant force when handling 10 μm to 1 mm parts even though Fig. 2.2 shows otherwise. That is because capillary forces can be eliminated by a dry or vacuum environment, if needed, and surface roughness is not so significant for electrostatic forces compared to van der Waals forces because the effective distance is longer.

Capillary forces due to surface tension have an effect on handling – that makes humidity controlling important in microhandling (Zhou et al., 2004; Jääskeläinen et al., 2009). The self-assembly part of the technique used in the experimental part of this thesis is based on capillary forces and they are discussed in more depth in Chapter 3.

All these types of adhesion forces not only disturb the microhandling process – they have also been exploited when new principles for handling micro-objects have been developed.

2.3 Different microassembly strategies

Three most commonly used microassembly methods are robotic assembly, self-assembly and wafer-level techniques (Cohn et al., 1998).

The robotic assembly methods use mechanics to achieve the desired position. Self-assembly processes use different principles to create energy minimum corresponding to the desired position. Wafer-level techniques include, for example, bonding and layer transfer. The wafer-level techniques can be used when the assembled objects are in same size scale. By bonding two wafers different cavities can be created. In the layer transfer techniques,

structures are first processed on one wafer by micromachining techniques and then bonded to another and detached from the original wafer. Wafer-level techniques are more like applications of microfabrication and they are not discussed more deeply in this context (Schmidt, 1998; Franssila, 2004).

Robotic assembly and self-assembly, as well as their pros and cons, are discussed in this section because the features of these two are combined in the experimental part of this thesis. The concept of hybrid method is presented and discussed in this section also.

2.3.1 Robotic assembly

Typical components of a robotic assembly setup are a microgripper, positioning system, sensors and control system. An example of a robotic assembly setup previously developed at TKK (Zhou et al., 2006b) is shown in Fig. 2.3.

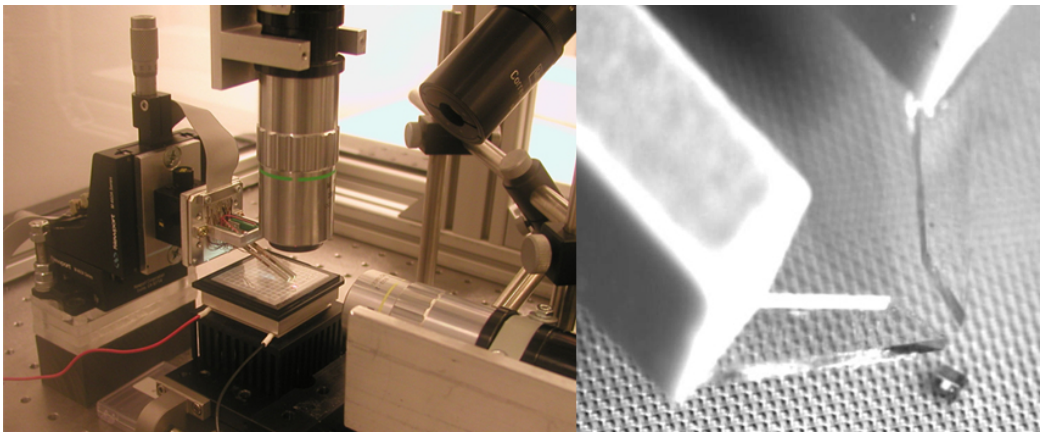

Figure 2.3: Left: A robotic assembly setup previously developed at TKK and a microgripper picking up a microchip.

Microgrippers are actuated with different principles, for example, the inverse piezoelectric effect (Haddab et al., 2000; Zhou et al., 2006b), the shape memory effect (Lee et al., 1996; Kohl et al., 2000), thermal expansion (Du et al., 1999; Chronis and Lee, 2005) and electrostatic force (Chu and Pister, 1994; Millet et al., 2004).

The positioning system is usually composed of linear and rotary precision stages based on various principles, such as DC motors, piezoelectric actu-

ators and piezoelectric motors. Piezoelectric actuators can provide higher resolution than DC motors. Positioning is often divided into rough and fine positioning systems so that speed and accuracy demands can be fulfilled.

Robotic handling is usually a serial process, containing pick-and-place operations. The main problem in robotic microhandling is adhesion between the tool and the part, also damaging of the parts is a problem. Different end-effectors have been developed to solve these problems. Fig. 2.4 shows schematics of some different *handling strategies*, which are next briefly introduced.

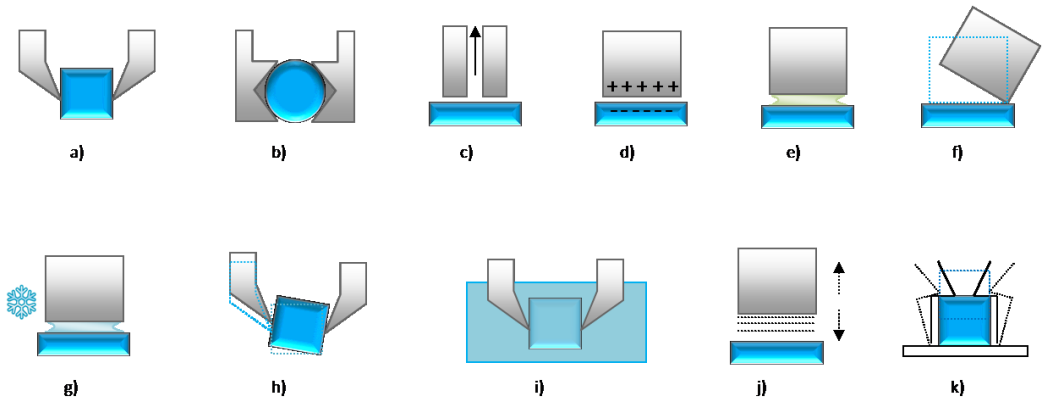

Figure 2.4: Different micromanipulation techniques: a) Contact microgripper; b) Form-closure microgripper; c) Suction gripper; d) Electrostatic gripper; e) Capillary gripper; f) van der Waals gripper; g) Ice gripper; h) Collaborative manipulation; i) Submerged micromanipulation; j) Vibration release; k) Snap-locking fixing (Zhou and Sariola, 2009).

The *friction based* handling strategy is also known in the macro world (contact microgripper). In the experimental part of this thesis, piezo actuated tweezers are used and they are discussed more carefully in Chapter 4. A gripper can be coated with conductive or hydrophobic materials to help the releasing procedure. A rough surface and vibrations of the gripper tips can also make the releasing easier.

With a *form closure gripper*, the place of the picked object can be determined in relation to the gripper, but objects that can be picked must have a specific form. A *suction gripper* uses a vacuum pump for picking; releasing is done with a puff of air (Bos et al., 2008).

Electrostatic force can also be used for picking. Potential is generated between the tip and the object to be picked. Releasing is done by shorting the electrodes or inverting the polarity (Tsuchiya et al., 1998; Fantoni and Porta, 2008). Capillary grippers are based on *surface tension*, the gripper being linked to the handled object by a liquid bridge. Releasing can be done with the help of e.g. hydrophobic coating, heating (drying), vibration or air pressure (Lambert and Delchambre, 2005; Fantoni and Porta, 2008). Capillary forces are more closely discussed in Chapter 3.

Feddema et al. (1999) proposed a handling strategy based on *van der Waals forces*. A part can be picked up simply by touching, and releasing is achieved by decreasing the common surface area between the gripper and part. *Cryogenic strategy* is an example of *phase change gripping* strategy, being based on the adhesive effect of frozen fluids. A small amount of liquid is frozen in between the tip of the gripper and the object to be handled. Releasing is done by heating the tip until the ice has melted. Handling can be done in air by adding the water with some actuator or in aqueous environment, where a submerged gripper exploits the liquid medium to generate an ice droplet (Kochan, 1997; Liu et al., 2004; López-Walle et al., 2008).

In *collaborative manipulation* two or more end effectors are used to make the handling more dexterous. An example is a 6 degrees of freedom microgripper developed at TKK. The gripper can translate the object it has picked in all three axis and rotate it in two axis (Zhou et al., 2006b). Collaboration in manipulation can also be an additional tool with a smaller contact area that is used to help in releasing.

Strategies for releasing which are unrelated to the gripping principle contain, for instance, *snap-locking* (see Fig. 2.5) (Dechev et al., 2004), vibrations and gluing the part on a substrate. In addition, controlling the environment reduces the effects of adhesion forces, for example, vacuum, low humidity or releasing in fluid (Zhou et al., 2004).

Other principles used in microhandling are, for example, *ultrasonic pressure*, *optical pressure* and the *bernoulli effect*. In the ultrasonic pressure principle acoustic waves are utilized to generate force. In the optical pressure principle

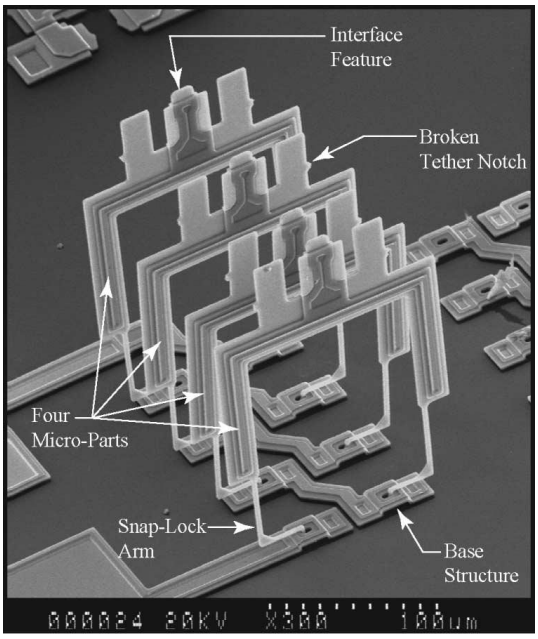

Figure 2.5: Releasing strategy: snap-lock (Dechev et al., 2004). Copyright ©2004 IEEE.

the visible radiation pressure of visible laser light is used to move small parts. The bernoulli effect is used to levitate parts – compressed air comes from the nozzle and after collision with the part it flows outwards. That evokes a dynamic pressure decrease and force upwards (Waltham et al., 2003; Vandaele et al., 2005).

Tichem et al. (2004) listed criteria that must be discussed when choosing a gripping principle. Sensitivity to adhesion forces is one criterion: as discussed before, adhesion forces are dominant in microscale. Accuracy in gripper-part relation is important: it does not matter how accurate kinematic modules the system has if gripping or releasing causes more error. Material type may be compulsory for some gripping principles, like ferromagnetic parts for a magnetic gripper, but it can be changed to some degree by adding coatings to the handled part. Surface properties (e.g. roughness) affect the gripping principle possibilities.

Force control is important, because fragile parts may be otherwise damaged by gripping. Moreover, the capability to produce enough force must be considered. Some gripping principles demand specific shapes for gripping to be successful, for example, a friction-based gripper needs two surfaces

on the side of the part. Different principles produce also different cycle times, and depending on the application, that may be important. The assembly environment also limits the choices – some principles demand certain environmental conditions (Tichem et al., 2004; Zhou et al., 2006a).

2.3.2 Self-assembly

Self-assembly refers to autonomous generation of order in systems of components without human intervention. It has its origins in chemistry – in molecular systems forming, for instance, crystals (Boncheva and Whitesides, 2005; Brammer, 2004). The fundamental working principle of the self-assembly techniques is the principle of minimal potential energy – the desired position must correspond the energy minimum of the system (Cohn et al., 1991; Sariola et al., 2008a).

In self-assembly the components to be assembled have to be mobile. Usually self-assembly is made in fluid phases or on smooth surfaces (Whitesides and Grzybowski, 2002). Autonomy enables parallel processes and large output, but local minima may cause assembled particles to become stuck, preventing them from going to the desired places. Excitation, such as vibration can be used to reduce such problems. Moreover, catalysts can be used – larger parts which are not taking part in the actual assembly can trigger the smaller parts to move when they hit each other during vibration (Baskaran et al., 2008). Another common practise in self-assembly is that more assembled parts than binding sites are used to help all sites to fill.

Gravity is a relatively weak force in microscale, but it can be used as a driving force for both fluidic and dry microassembly. In fluidic gravity driven assembly, the fluid transports the assembled parts near the micromachined wells and gravity takes care of the placement and orientation (Cohn et al., 1991; Yeh and Smith, 1994; Morris et al., 2005). In dry assembly, gravity can be used in the same way, but transport can be done by shaking or vibrating the plate. A result of one dry assembly process can be seen in Fig. 2.6 (Fang and Böhringer, 2006).

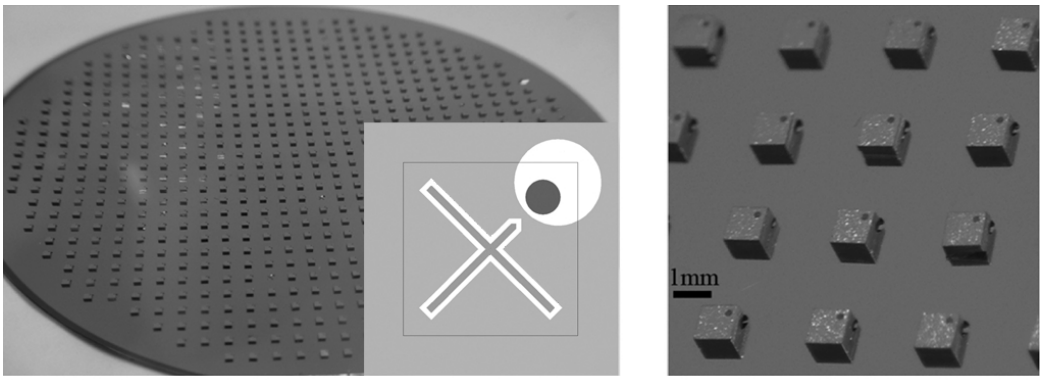

Figure 2.6: Dry self-assembly results with shape recognition method. The drawing shows the exact alignment between the receptor site and the part (Fang and Böhringer, 2006). Copyright ©2006 IEEE.

Capillary force can be used as a driving force in self-assembly – it results from a surface tension of a meniscus (a liquid bridge between two objects). The binding sites are either hydrophobic or hydrophilic depending on whether the assembly is performed in water or in air. Because capillary self-assembly is a part of the technique used in the experimental part of this thesis, its theory and applications are discussed more deeply in Chapter 3.

Magnetic, electromagnetic or electrostatic forces can also be exploited (Whitesides and Grzybowski, 2002). Figure 2.7 shows the schematics of an electrostatic assembly method.

2.3.3 Hybrid assembly

Some microhandling strategies contain both robotic and self-assembly characteristics, the distinction between the two branches is no more clear. For example, potential trapping is the base of the self-assembly methods, but can be exploited also with robotic methods. The capillary gripper can benefit from self-assembly – when picking with fluid the surface forces can align the micropart to the head of the gripper (Bark et al., 1998).

The method used in the experimental part of this thesis is a hybrid method. A microgripper is used to carry the parts near the desired position and the final alignment is done with the help of capillary forces by dispensing a water

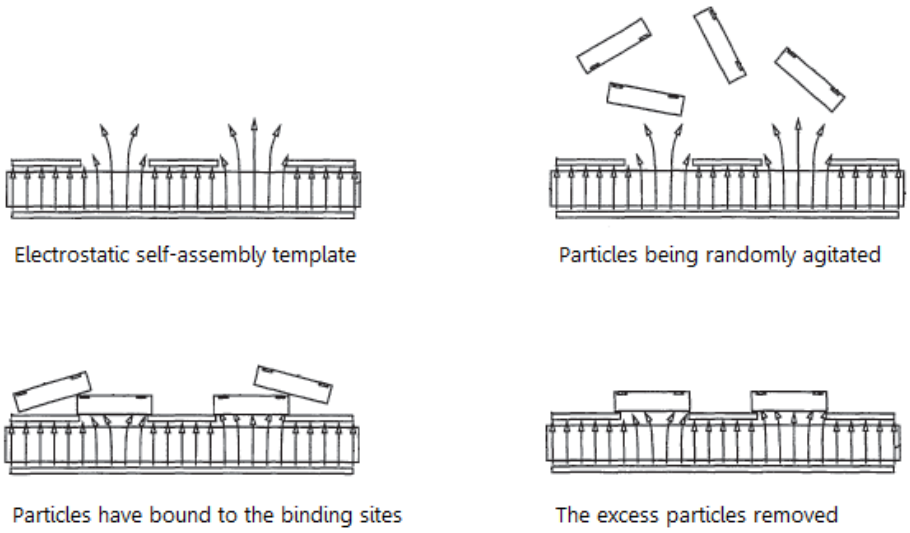

Figure 2.7: Dry electrostatic self-assembly. Adapted from Cohn (1994) with permission.

droplet on the receptor site before the releasing. The capillary force between the part and the receptor site also prevents the part from sticking on the gripper tips. Details of the method and apparatus will be described later.

Sariola et al. (2008a) listed elements that any microhandling strategy can benefit from:

- Potential trapping
- Ambient environment
- Disturbance rejection
- Perturbation
- Surface and material properties
- Hierarchical positioning

Some of those elements are more related to self-assembly and others to robotic assembly. However, if this division is put aside and the development process of new methods is started with a clean slate with these elements, many new hybrid methods will arise. The desirable characteristics of both self-assembly and robotic methods can be combined and exploited.

Chapter 3

Capillary Forces in Microhandling

As discussed in Chapter 2, adhesion forces may have a strong effect in microhandling. One of the adhesion forces is capillary force, which may, for example, cause the handled object to adhere to the tips. These unwanted effects of the environment can be reduced by material selection and by controlling the humidity.

Capillary forces can also be used in a controlled way for the gripping and handling of micro objects. This chapter discusses first the physics behind capillary forces and then some different applications of capillary forces in microhandling.

3.1 Physics

3.1.1 Surface tension

Surface tension is a property of liquids. It is caused by attractive forces between the molecules of a liquid. Inside the liquid the net force is zero, because the molecules are equally attracted from every direction. At the surface the attraction is larger from the inside of the liquid. This makes

the energetic state of the molecule less favorable at the surface and leads to minimization of the interface area. This difference is illustrated in Fig. 3.1. This surface energy approach considers surface tension as units of energy by surface unit (J/m^2). Another approach to surface tension is to consider it as a tensile force by length unit (N/m).

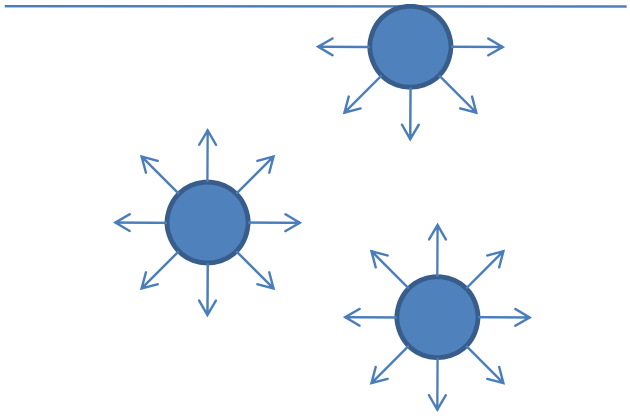

Figure 3.1: Surface tension. Molecules are attracted by neighboring molecules.

Surface tension (γ) leads to a pressure difference, which is linked to the curvature of the interface (H, mean surface curvature), because surface tension forces attempt to cancel the force due to pressure. Equation 3.1 shows this relation and is called the Laplace equation. P_{int} stands for the pressure on the internal side of the surface and P_{out} stands for the pressure on the external side.

$$P_{int} - P_{out} = 2\gamma H \tag{3.1}$$

3.1.2 Contact angle

The contact angle (θ) is the angle between the liquid droplet and the solid surface. With ideal surfaces the contact angle in equilibrium can be determined from the force balance, from the Young-Dupré equation (3.2).

The subscripts of surface tension (γ) refer to liquid (L), vapor (V) and solid (S).

$$\gamma_{LV} \cos\theta + \gamma_{SL} = \gamma_{SV} \tag{3.2}$$

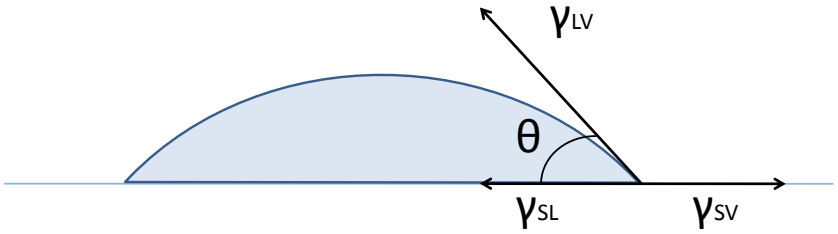

Figure 3.2: A droplet on solid surface at the equilibrium.

The contact angle is a measure of wetting properties of a surface. Surfaces with contact angle smaller than 90° are called *wettable* (if the liquid used is water the term is *hydrophilic*) and surfaces with a contact angle larger than 90° are called *non-wettable* (*hydrophobic*). In Fig. 3.3 there is an example of a droplet on different surfaces. On the left, the surface is more hydrophilic than on the right. In practice the angle is not exactly from the Young-Dupré equation (3.2), but is maximum for advancing liquid edge and minimum for receding liquid edge. That is called contact angle hysteresis. The surface properties and contact angle can be changed by using different materials or by modifying the surface roughness (Torkkeli, 2002).

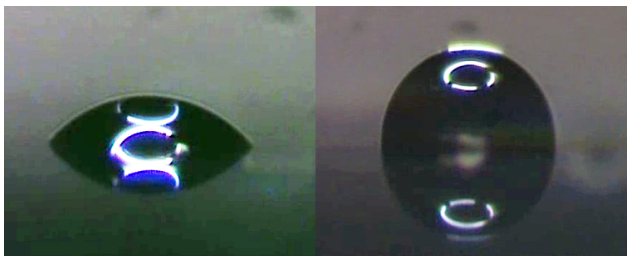

Figure 3.3: An example of a water droplet on different surfaces: on the left the surface is more hydrophilic than on the right.

In capillary force assisted microhandling, the wetting properties are important. Wetting characteristics of the components and the substrate define the final positions of the components in the capillary self-assembly process.

Differences in the wetting properties of the surfaces can be used to control the assembly process to obtain desired assemblies. Some examples are discussed later in the context of applications of capillary forces in microassembly.

3.1.3 Liquid bridge – meniscus

The term meniscus is used in this thesis to refer to a liquid bridge linking two solids. The physics of the meniscus and capillary force are briefly introduced in this section which is mainly based on the study of Lambert (2007). The solid is submitted to *capillary force* F_C, which is the sum of two force components, *Laplace force* F_L and *tension force* F_T. The equations of these two force components are given in an axially symmetric case between two parallel plates (see Fig. 3.4).

$$F_C = F_L + F_T \tag{3.3}$$

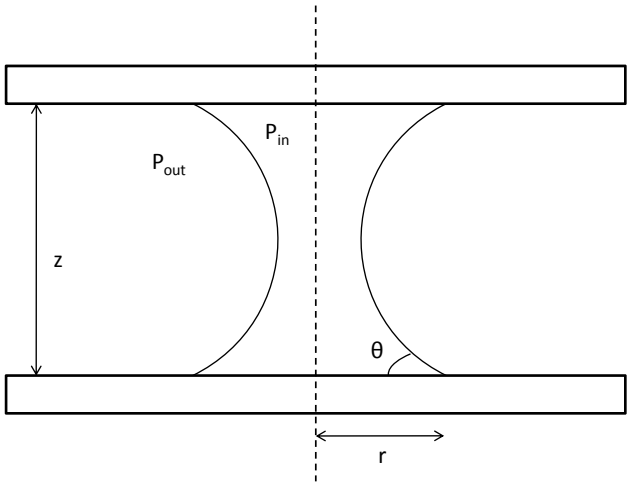

Figure 3.4: Meniscus between two plates.

Pressure difference (see Equation 3.1) leads to the Laplace force, which in an axially symmetric case is acting over a contact circle (radius r) between the object and meniscus. This force can be repulsive or attractive depending on

the shape of the meniscus: a concave meniscus leads to an attractive force and a convex meniscus leads to a repulsive force.

$$F_L = 2\pi r^2 \gamma H \tag{3.4}$$

Another component of capillary force is the tension force, which is always attractive. That force is the integral of the surface tension projected on the vertical direction. Equation 3.5 shows the force when the meniscus is axially symmetric between two plates.

$$F_T = 2\pi r \gamma \sin\theta \tag{3.5}$$

For calculating the components of the capillary force, the meniscus geometry, materials and liquid properties must be known. In more complex geometries some approximations must be done. Lambert (2007) presents a comprehensive study on different geometrical approaches to estimate the capillary force including, for instance, circle approximation, where the meniscus is approximated by an arc, and the double iteration approach. The double iteration approach intends to obtain the exact shape of the meniscus from the differential equation:

$$2H = \frac{r''}{(1+r'^2)^{3/2}} - \frac{1}{r(1+r'^2)^{1/2}} \tag{3.6}$$

A comprehensive comparison of the arc approximation and the double iteration approach can be found in Chang et al. (2007). Methods are compared in different system parameters for several configurations. Fig. 3.5 shows the difference between the methods as a function of contact angles when the capillary force between two parallel plates is calculated. It shows the problem of the arc approximation method: the contour of the liquid turns to be a straight line when the sum of two contact angles is 180 degrees. The error becomes large. However, in general, if the limitations and assumptions of different approximations are known and taken into account, they can be used in the calculation of capillary force.

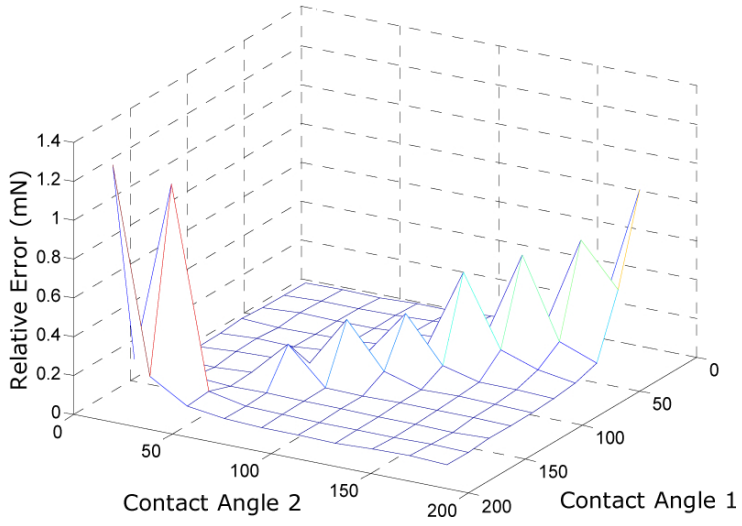

Figure 3.5: Relative error between arc approximation method and the double iteration method (Chang et al., 2007).

Another way to estimate the capillary force is to use an energetic approach. At first *the total surface energy* W is calculated as a sum of surface energies in a solid-gas interface, solid-liquid interface and liquid-gas interface. To be able to calculate the capillary force, the shape of the meniscus is approximated and the volume of the liquid is assumed to be constant. After these assumptions the force can be calculated as a derivative of W in respect to z (separation distance).

$$F_z = -dW/dz \tag{3.7}$$

The free energy in a self-assembly system is directly proportional to the area of hydrophobic or hydrophilic surfaces depending on whether the assembly is performed in water or in air. The free energy is lowered when these surfaces meet. That energy gain is proportional to the overlap of the regions. If the same hydrophobic/hydrophilic coating is assumed in those regions, the surface energy can be approximated ($\gamma_{\pm}$ is the interfacial energy of all hydrophobic/hydrophilic interfaces) (Böhringer et al., 2001):

$$W = -2\gamma_{\pm} \cdot |A \cap B| \tag{3.8}$$

Equation 3.8 is used to demonstrate the surface energies of a system where a square part is assembled on a square binding site. Fig. 3.6(a) shows that when the angular error is assumed to be 0°, there is only one global minimum for W which corresponds to the part matching exactly the binding site. Fig. 3.6(b) shows the effect of symmetry: part symmetry leads to four possible assembly orientations, which correspond to the minima of the energy curve.

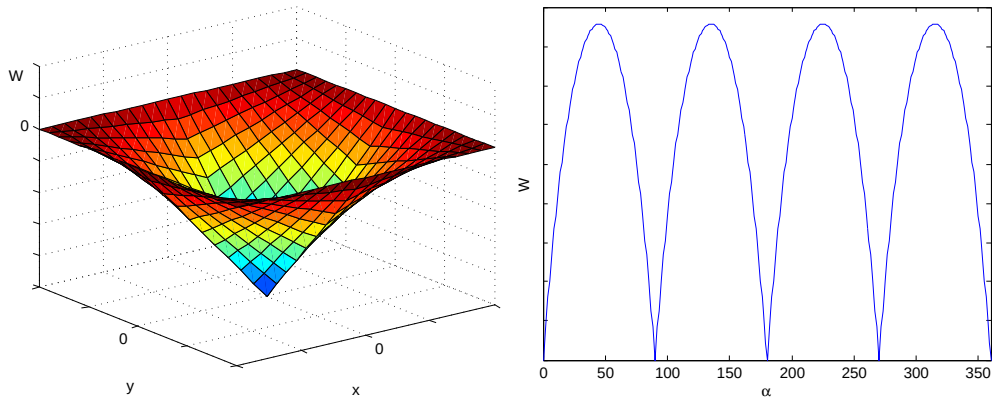

(a) W plotted against x and y with 0° rotation

(b) W plotted against rotation angle α, (0,0,α)

Figure 3.6: Surface energy W of a square part and binding site.

The Surface Evolver (Brakke, 1992) is a program for minimizing surface energies subject to constraints. The surface is approximated with triangles and the gradient descent method is used for evolving the surface with minimal energy with, for example, constant amount of liquid. Fig. 3.7 shows an example of a sphere with minimal surface energy evolved from a volume determined by the cube.

Both the Laplace method and the surface energy method approaches give equal results. In axially symmetric cases, the Laplace method with geometric approximations is better because it is easy to solve. When full 3D geometry is needed, the energetic method is preferred.

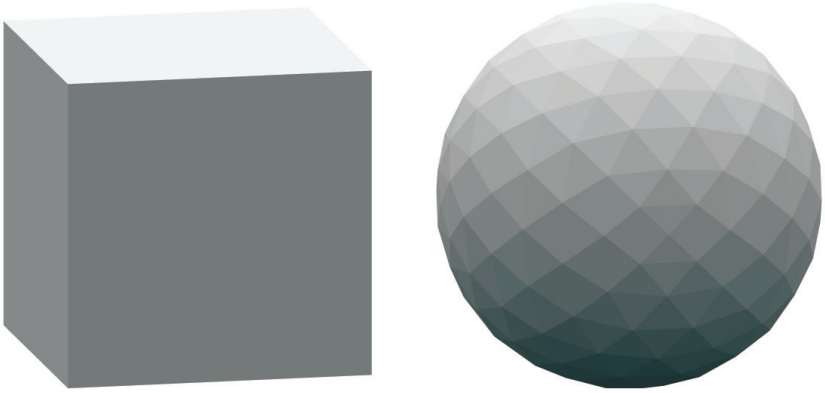

Figure 3.7: Cube on the left prescribes the volume, which evolves into a sphere with minimum surface energy (generated using The Surface Evolver).

3.2 Applications of capillary force in microhandling

3.2.1 Capillary self-assembly

Capillary force can be used as a driving force in self-assembly, which is caused by surface-energy minimization. Traditionally, the self-assembly process is stochastic: in parts to each other and in part to template assemblies the overall configurations is determined in advance, but the positions of individual parts are random and not predefined. The final positions may be defined more accurately with hybrid methods where the rough alignment is done by some other method and capillary forces are used for final alignment. One such method is used in the experimental part of this thesis and is discussed more deeply in the next chapter.

In capillary self-assembly the capillary force resulting from the surface tension of the meniscus is used as a driving force. The receptor sites used to control the assembly process are either hydrophobic (non-wettable) or hydrophilic (wettable). In an aqueous environment, the receptor sites are hydrophobic for acrylate-based adhesives or hydrocarbon liquids. In air the hydrophilic receptor sites are used for water based fluids. If molten solder is used, the receptor sites are coated with thin metal films having good solder-wetting properties (Saeedi et al., 2006; Mastrangeli et al., 2009).

Capillary self-assembly can be driven by fluids or with e.g. molten solder. One advantage of molten solder driven assembly is that electrical and mechanical connections are made at once. Material properties limit the choices, because molten solder driven assembly cannot be applied to temperature sensitive surfaces. In fluid driven assembly the liquid used must be chosen so that is does not damage the assembled parts. Sometimes the receptor sites may also be damaged during the alignment process because of the freely moving parts (Mastrangeli et al., 2009).

Assembly to construct 2D and 3D arrays and structures

Capillary force can be exploited when parts are assembled to each other to construct different structures and arrays in 2D and 3D. Systematic research of the topic has been carried out since the 1990s. Green et al. (1995) demonstrated the use of capillary force to produce out of plane rotation with molten solder (see Fig. 3.8). After the solder is placed it is heated to its melting point, and when the liquid minimizes its surface energy the plate is pulled away from the substrate.

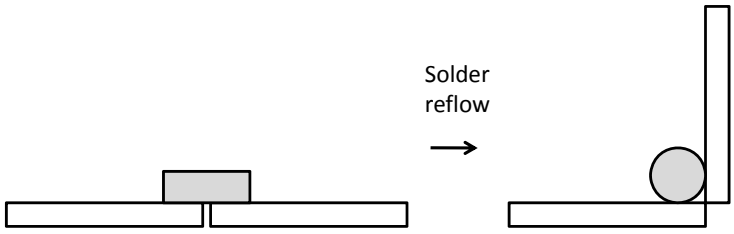

Figure 3.8: Out of plane rotation with molten solder.

Different 2D and 3D structures can be assembled also by floating the parts in liquid-air or liquid-liquid interface. The idea is adopted from molecular self-assembly and is based on shape-selective recognition of surfaces and minimization of interfacial free energies (Terfort et al., 1997). Denkov et al. (1992) reported the mechanism of array formation from micrometer-size latex particles on glass. Later mm-sized hexagonal plates, cubes and key- and lock structures with different combinations of hydrophilic and hydrophobic edge faces have been assembled into various ordered arrays (Bowden et al., 1997) and the same group assembled also submillimeter objects sizes ranging from 0.1 mm to 10 mm (Grzybowski et al., 2001).

Complicate 3D structures have been assembled by self-assembly. Gracias et al. (2000) reported assembly of millimeter-scale polyhedra forming electrically functional, three-dimensional networks. An example of those assembled aggregates can be seen in Fig. 3.9.

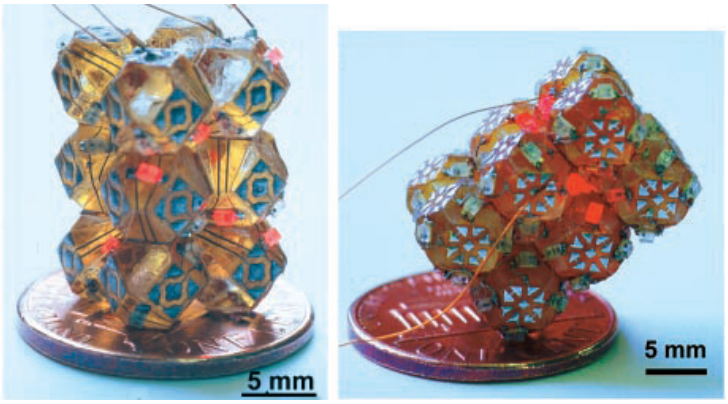

Figure 3.9: Self-assembled aggregates (Gracias et al., 2000). Reprinted with permission from AAAS.

Part to template assembly

In the part-to-template assembly process, the receptor sites on the assembly template are covered with a liquid or with molten solder. As the assembled parts get introduced to the assembly template, they attach to the receptor sites and self-align over the sites to minimize the surface energies. Many groups have studied the part-to-template assembly with artificial test parts (for example, Sato et al. (2003); Srinivasan et al. (2001)) and also real components have been used, for example, PZT actuators, LED components and optical components (Fang et al., 2005; Avital and Zussman, 2006).

Srinivasan et al. (2001) used hydrophilic-hydrophobic patterning of the surface and adhesive liquid to drive the assembly process. Many different *binding site geometries* were studied, for example, circles, rectangles, rings and commas. 100 % yields were attained with symmetric patterns, but with multiple possible assembly orientations (a rectangle has two different possible orientations and a circle has an infinite number of possible orientations). To eliminate those numerous minima the asymmetric comma shape was studied.

However, the local minimum was still observed. In this study part sizes ranged from 150 µm x 150 µm x 15 µm to 400 µm × 400 µm × 50 µm.

Another study to obtain unidirectional self-assembly was carried out by Lin et al. (2007) – for example, teardrop shaped patterns were designed. That pattern was further developed and a tear-drop pattern with an elliptical hole was studied (Lin et al., 2009). 100 % unidirectional assembly yield was achieved with the tested 1100 µm × 1100 µm × 440 µm part. Examples of some shapes used in the self-assembly are roughly presented in Fig. 3.10.

Figure 3.10: Different shapes used as self-assembly patterns. Three on the left adapted from Srinivasan et al. (2001), and the two on the right adapted from Lin et al. (2007, 2009).

The possibilities of *water steam* are mentioned by Fang and Böhringer (2006). Their semi-dry assembly process (semi-DUO-SPASS) uses capillary self-alignment for final alignment by adding water steam after rough alignment. Rough unidirectional alignment is achieved by anchoring the parts by gravity and trenches of the receptor sites before the water steam was added. The method was demonstrated using 2 mm square silicon parts.

Another option for determining the final position of the part is to use *solid edge* instead of hydrophilic-hydrophobic patterning. The method used in the experimental part of this thesis utilizes solid edge in assembling a micropart on top of another (del Corral et al., 2003) and is better described in the next chapter. The advantages of the solid edge include less friction and less overflow of the liquid when compared to surface treatment alone (Tsai et al., 2007).

Heterogenous assembly is needed when different microparts are assembled on the same assembly template. One method is multiple batch assembly presented by Xiong et al. (2001). Gold patterns are used as binding sites and they are activated with hydrophobic alkanethiol self-assembled monolayer (SAM). For each batch of microparts, only the desired binding sites on the substrate are activated by desorption of SAM from undesired sites.

The assembly itself is done by adding lubricant to the template and then immersing the template in water, where the lubricant forms droplets on the receptor sites. The parts in the water align to the sites. After curing the lubricant by heat the adsorption and the desorption of SAM can be done again for new batches. Moreover, programmable surface chemistry has been proposed to be an option for multi-batch assembly (Böhringer, 2003).

Stauth and Parviz (2006) present another method for heterogenous assembly (Fig. 3.11). *Shape recognition* (see also Yeh and Smith (1994)) and gravity are used to help the components in fluid to find the proper receptor sites. Capillary forces between molten alloy on template then make the components to align and to connect electrically with the substrate. In that way many different components can be assembled simultaneously and no multiple batches are needed. In the experiments, yields of 97 % for components as small as 100 µm have been achieved.

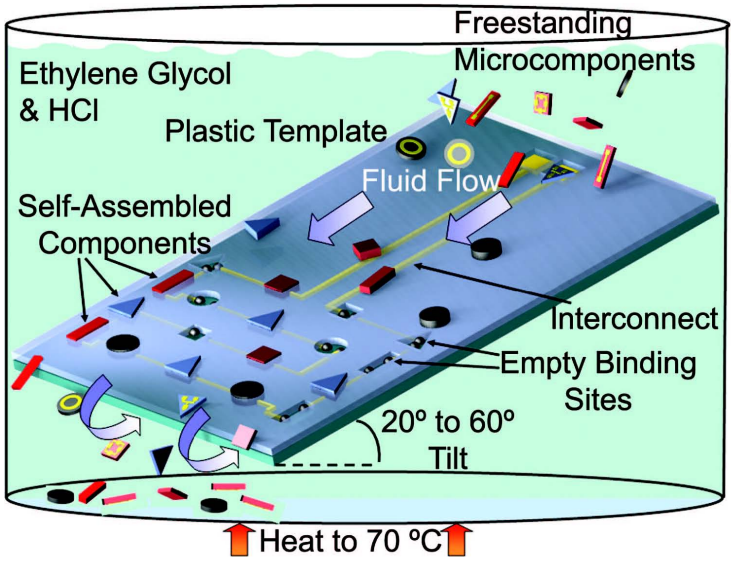

Figure 3.11: The heterogeneous self-assembly process (Stauth and Parviz, 2006). Copyright ©2006 by the National Academy of Sciences.

Local minima cause difficulties in the self-assembly process. Tilting of the microparts (part not parallel with the assembly template) has been reported, especially when the amount of liquid is large. Abbasi et al. (2008) shows that vibrating the plate helps in tilt correction by giving external energy to the system. However, tilting of the parts is considered less a problem than shift (lateral) and twist (angular) displacements. Surface energy increases rapidly

even with small tilt angles but with shift the restoring force decreases near the perfect alignment, especially when the amount of liquid is large. This alignment force softening appears also with twist displacement and it makes small errors possible (Greiner et al., 2002). To reach the perfect alignment the parameters of the process have to be evaluated and studied accurately.

3.2.2 Capillary grippers

As discussed in Chapter 2, the adhesion forces can be exploited as a gripping principle. Capillary force is very effective in microscale and has been considered as a possible gripping principle by many authors (Bark et al., 1998; Grutzeck and Kiesewetter, 2002; Obata et al., 2004).

The capillary gripper is based on a meniscus between two surfaces: the surface of the gripper and the surface of the object to be gripped. A droplet is applied to the surface of the gripper before gripping and when there is a contact between the droplet and the object to be gripped, the capillary forces make the object adhere to the gripper (see Fig. 3.12).

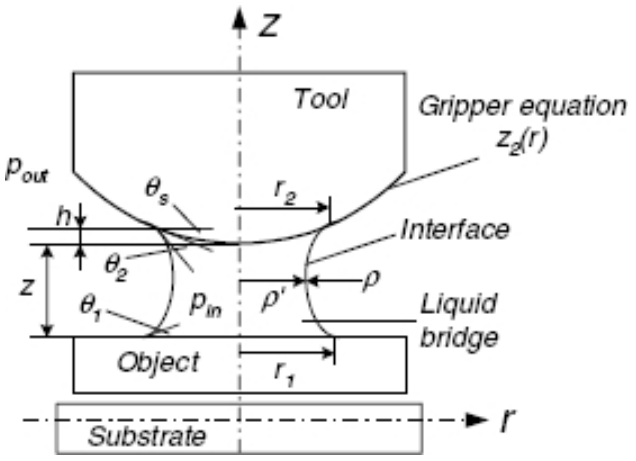

Figure 3.12: Capillary gripper (Lambert and Delchambre, 2005). Copyright ©2005 IEEE.

Lambert and Delchambre (2005) present a thorough study on design rules of a capillary gripper. In *picking* there are five aspects to consider: contact angles of the used materials, surface tension properties of the liquid, the gap (z), volume of liquid used and the gripper's geometry.

Contact angles depend on the material of the gripper and the object but also on the liquid used. To increase the force the contact angle between the object to be gripped and the liquid must be small. However, it must be taken into account that liquids with too low surface tension cannot be used even if they have better wetting properties, because the force that the liquid bridge produces is proportional to surface tension.

The adhesion force is maximum when the gripper and object are touching and decreases when the gap increases. The gripper's geometry affects directly the force but also through the volume of the liquid. With different geometries, the relation between the force and the volume of the liquid is different (Lambert and Delchambre, 2005).

Releasing can be done through evaporation of the liquid but sometimes other methods are needed because other adhesive forces are also affecting between the gripper and object. The gripper can be tilted similarly as in a handling strategy based on van der Waals forces to reduce the contact area or the gap can be increased (Feddema et al., 1999; Lambert and Delchambre, 2005).

The geometry of the gripper has a strong effect in releasing also. Releasing can be done by modifying the geometry. Also, dynamical effects such as acceleration can be used to facilitate the releasing (Lambert and Delchambre, 2005). Vasudev and Zhe (2008) demonstrated the use of electrowetting (controlling of the contact angle by a voltage) in the releasing process.

An advantage in capillary gripping is that the gripped object may self-align to the gripper, which makes gripping very precise. Very high forces can be obtained but the gripping process is still very gentle (Grutzeck, 2005).

Chapter 4

Experimental Design

4.1 Overview of the method

The hybrid handling method used in this study combines robotic handling and capillary self-assembly. A microgripper is used for rough positioning and the final alignment is done by capillary forces. The tweezer-type microgripper takes a micropart, *a top part*, near the receptor site – in this study the receptor site is another part, *a bottom part*. A water droplet is dispensed between the parts and when the top part contacts with the droplet a meniscus is formed. The principle of minimum potential energy makes the parts align by capillary force. The principle of the method is shown in Fig. 4.1.

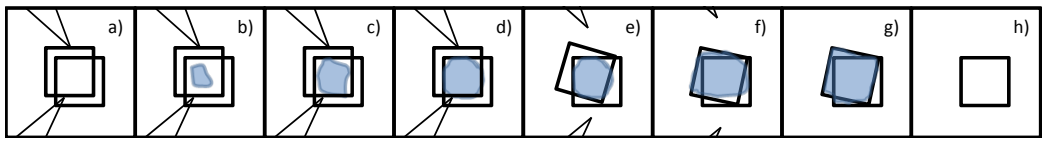

Figure 4.1: Hybrid handling method: a) Microgripper approaches the releasing site with a part b) A droplet of water is dispensed between the microparts c) The droplet contacts with the top part and starts to wet d) Wetting is finished e) The microgripper opens, releasing the part for self assembly f and g) The capillary force aligns the top part to the bottom part h) The water between the two parts evaporates, leaving the two parts aligned.

The method was developed at TKK and it was presented for the first time by del Corral et al. (2003) with 300 µm × 300 µm parts. Also Sato et al. (2003) and Tsai et al. (2007) use a similar hybrid method, but the surface area of the assembled parts is notably larger: 1 mm × 1 mm. Sato et al. (2003) use a patterned surface to constrain the liquid, while in Tsai et al. (2007) RFID-tags are assembled on a protrusion.

4.2 Experimental set-up

4.2.1 Microgripper and kinematics

The handling is carried out with a microgripper developed earlier at TKK (Albut et al., 2003). It is actuated with two 1 DOF bimorph piezoelectric benders. The gripper tips are stainless steel and can be aligned in 3 directions with manual stages. The gripper is on the left in Fig. 4.2.

A z-axis motorized stage (Physik Instrumente/M-111.1DG) is used to lower and lift up the gripper. Two translational precision positioning stages (model/manufacturer: Physik Instrumente/M-111.1DG) are used to move the part carrier in the x- and y- directions. The minimum incremental motion of the stages is 0.05 micron, the travel range of the stages is 15 mm and the unidirectional repeatability is 100 nm. Rotational encoders are used to measure the displacement of the stages. The same wafer that was used in the fabrication of SU-8 parts serves as a part carrier on the top of a Gel-Pak Vacuum release tray attached to the stages.

4.2.2 Dispenser

The dispenser used in the test is a non-contact dispenser (GESIM/PicPIP) actuated by a piezoelectric diaphragm (on the right in Fig. 4.2). The size of one droplet is approximately 0.1 - 0.5 nl and can be adjusted by controlling the actuation voltage and the pulse width. Larger droplets can be produced by dispensing several droplets.

4.2.3 Observing

The processes of dispensing, releasing and self-alignment (SA) are recorded with a top microscope (Edmund Optics/VZM-1000i) with a high speed charge-coupled device (CCD) -camera (Imperx/IPX-VGA210-G). There is a halogen fiber optic illumination integrated into the top microscope. A side view of the process can be observed with a side microscope (Edmund Optics/VZM-1000i) and a normal speed CCD-camera (Sony/XC-003P). There is also one overview microscope showing the overview of the area. The final accuracy of the tests is determined with a scanning electron microscope (SEM) (JEOL/JSM-840), where the samples are coated with gold in a sputter coater (Cressington 108 AUTO).

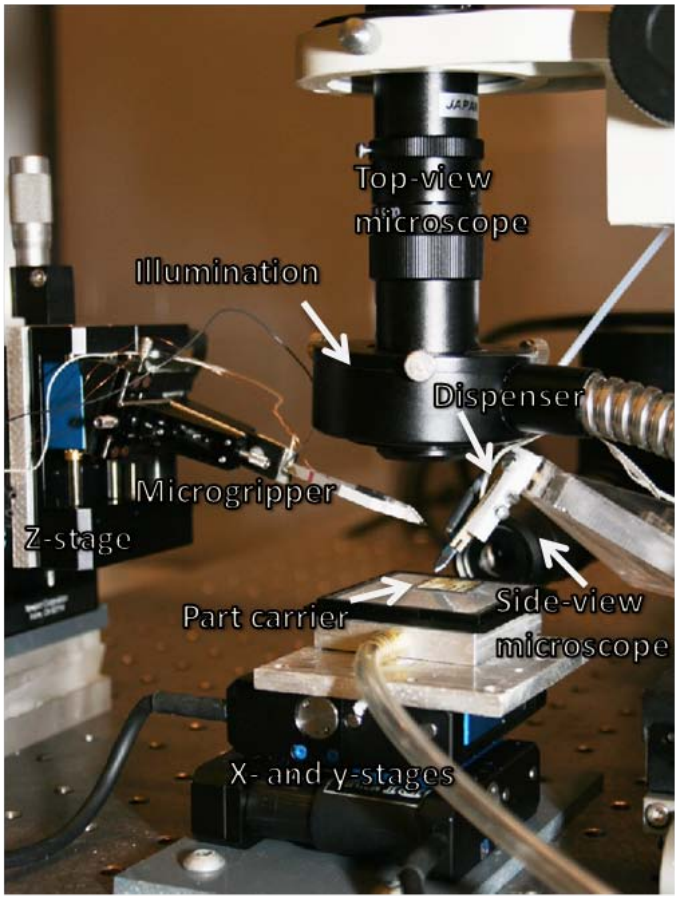

Figure 4.2: Hybrid microhandling set-up: top view and side view microscopes, the microgripper on the left and the dispenser on the right.

4.2.4 Environmental control system

The environment has an effect on microhandling, therefore, in all the tests the temperature and humidity are kept constant, at 25°C $^{\pm}$ 1°C and 45% $^{\pm}$ 1%. The tests are performed inside an environmental chamber developed previously at TKK (see Fig. 4.3). Temperature and humidity inside the chamber can be controlled with a custom-order controller from Arctest Oy.

Figure 4.3: Environmental chamber.

The walls of the chamber and the ceiling are double layered boards made of transparent polycarbonate and separated by air gaps. The walls are fixed on an aluminum structure. One sidewall of the chamber is connected to the environmental controller through an air inlet and an air outlet. The chamber and vibration isolation table (Newport VH) are separated by a thermal isolation layer. There is an air duct, an air buffer and a diffusion plate generating good air circulation. A filter in the air inlet keeps the air clean of particle sizes larger than 0.1 µm.

Temperature can be controlled between -10 and 40 °C and humidity between 5-85% RH. A detailed description of the environmental control system can be found in Zhou et al. (2004).

4.2.5 SU-8 microparts

SU-8 microparts are fabricated on a silicon wafer. First an aluminum layer is sputtered on the top of a clean wafer, then a layer of SU-8 (epoxy-based negative photoresist) is applied and patterned using lithography. Moreover, the parts are hard baked (Tuomikoski et al., 2003).

A piece of the wafer that contains the parts is treated with high humidity and heating so that parts can be easily detached. The piece of wafer is heated with a Peltier element that is fixed to a metal frame and driven by a voltage source. Humidity is produced by a humidifier (Bionaire Ultrasonic Compact BU1300W-I) where a tube is used to direct the steam to the piece of wafer. The temperature of the piece is 50 °C for 10 minutes, and then the piece of wafer is kept in high humidity for 10 minutes (almost 100% humidity can be assumed). The same is repeated and finally the parts are held at 60 °C and high humidity at the same time for 30 minutes. Some other methods were tested as well, but they were not successful: for example, using higher temperatures and boiling water.

4.3 Objective

The objective of the experimental tests is to study the influence of the sizes of the SU-8 microparts, the number of droplets and the bias (the difference between the release position and the final position) on droplet self-assembly based hybrid microhandling.

Firstly, the assembly of two microparts of the same size is studied, where two different sizes of microparts are used: 100 µm × 100 µm × 70 µm and 300 µm × 300 µm × 70 µm. These are illustrated in the two first images of Fig. 4.4.

It has been proven that it is possible to align a small part on the edge of a larger micropart (Sariola et al., 2008b). This phenomenon is investigated more systematically with the tests with parts of different sizes where the goal is to align a 300 µm × 300 µm × 70 µm micropart on the edge of a larger

part (300 µm × 600 µm × 70 µm), as illustrated in the last image of Fig. 4.4.

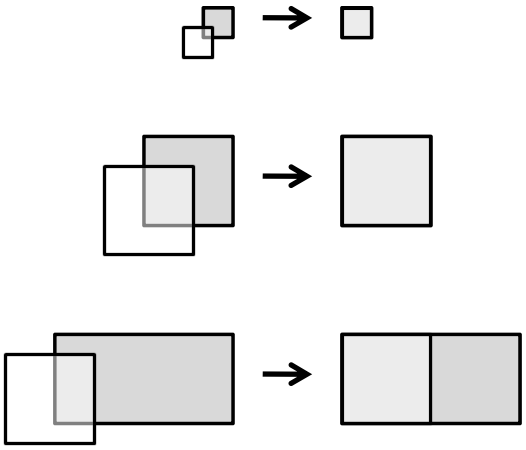

Figure 4.4: Different handling tasks.

In the previous studies of this method the droplet has been dispensed to the geometrical center of the bottom part, in other words to the center of the final position (Sariola et al., 2008b). In the tests reported in the following part of this thesis, the dispensing position is the geometrical center of the part to be released. These two approaches are shown in Fig. 4.5.

In the field of robotic microhandling the latter approach could be easily adopted: the bias means the initial positioning error of the part in releasing which affects both the releasing position of the part and the target of dispensing, if the dispenser and the gripper were fastened together. The results of the tests with these two different dispensing positions are compared in Chapter 5.

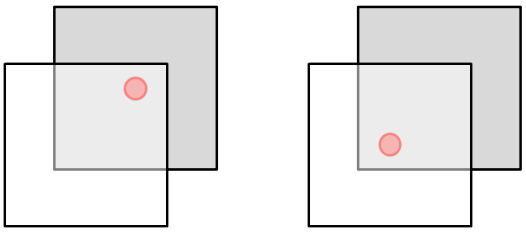

Figure 4.5: Different droplet landing locations when top part is in releasing position; left: the geometrical center of the bottom part, right: the geometrical center of the releasing position.

4.4 Success and failure – definitions

The success or the failure of one test can be determined after the motion of the top part ends. Based on observation, self-alignment is observed to be quite a binary process – failure and success can usually be easily detected from microscopic images. *Success* is defined when parts are aligned (Fig. 4.6) and failure is defined when there is misalignment (Fig. 4.7). In successful cases the energy minimum is found and capillary force aligns the parts. In failure cases the part is stuck at a local minimum or in some cases it adheres to the gripper tips or flies away during releasing.

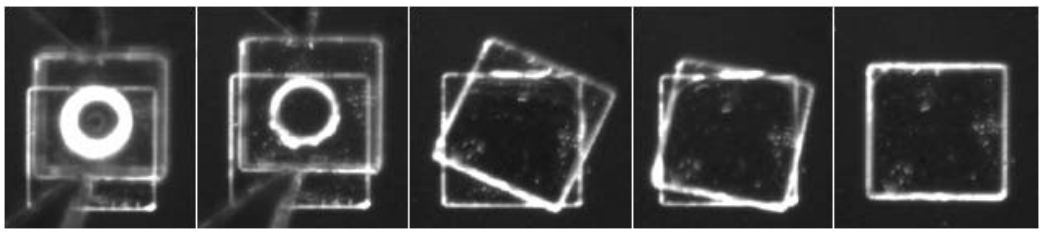

Figure 4.6: Successful self-alignment.

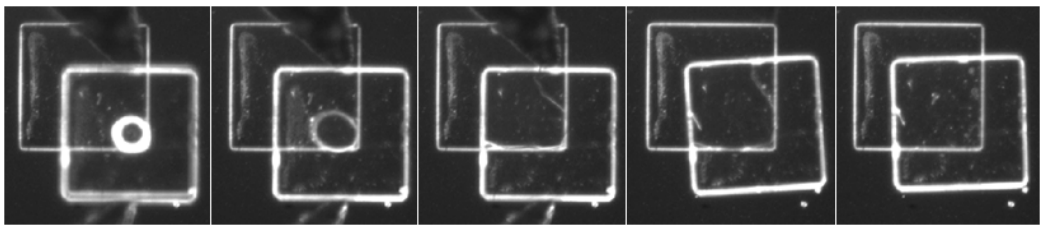

Figure 4.7: Failed self-alignment.

In the case of parts of different sizes, there are two possible places where a successful self-assembly can end. *A success* is when the top part aligns on the short edge of the micropart as in Fig. 4.8(a) and *a partial success* is defined to be the top part aligned somewhere else as in Fig. 4.8(b). *A failure* contains misalignment as defined in the case of the parts of the same size.

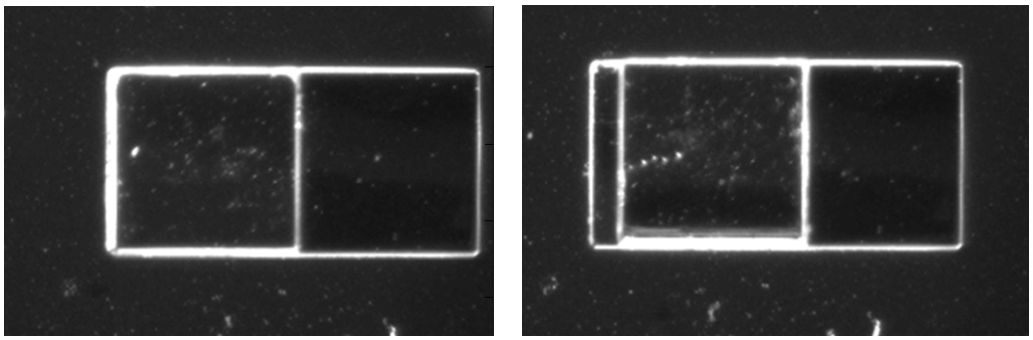

(a) Success (b) Partial success

Figure 4.8: Parts of different sizes have one option more.

4.5 Parameters

4.5.1 Amount of water

The effect of different amounts of water was tested by dispensing 1-20 droplets in the case of the 300 µm × 300 µm parts and 1-4 droplets in the case of the 100 µm × 100 µm parts, where the number of droplets is chosen randomly for each test. The parameters for the dispenser are the actuation voltage 40 V, and pulse width, 30 µs which should produce 129 pl per droplet according to the specifications of the dispenser.

During the tests it was noticed that there might be daily variations in droplet size, where the difference was not great but sometimes observable. The reason for that might be that the dispenser has been in use for quite a long period of time and the absence of clean room environment naturally affects the results. Such fluctuation was compensated for by calibrating the droplet size from the top view of a microscope image using a transparency where the size of the original droplet was drawn and the parameters of the dispenser is modified such that the size of the droplet matches the reference size. By using that method the amount of water could be kept roughly the same.

After the basic tests, however, a more sophisticated way of calibrating the droplet size was developed for future testing (see Fig. 4.9). A circle is fitted to the side view image of a droplet, then the intersections of a circle and the

part surface are defined and the volume of the spherical cap is calculated. This method was used after the batch of tests reported in this thesis to estimate the exact amount of water used. The estimated size of the droplet is about 170 pl.

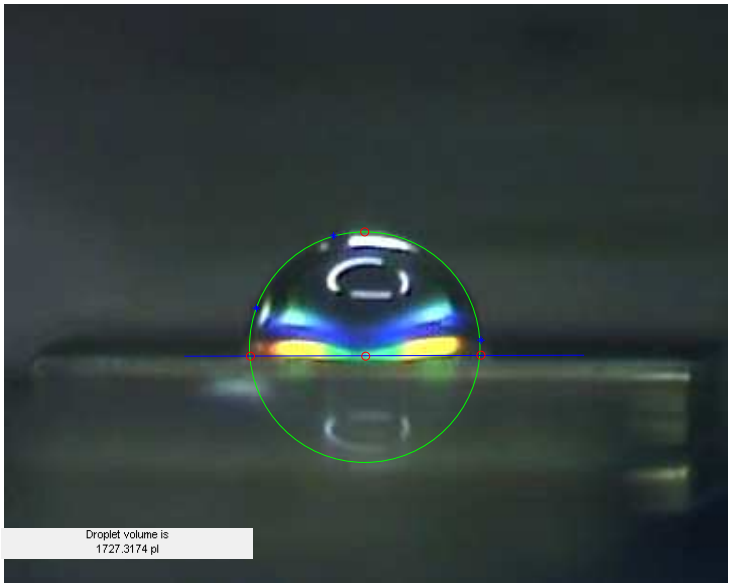

Figure 4.9: Droplet size estimation, 10 droplets burst.

In the tests with the smaller microparts, one droplet is already quite a lot of water related to the size of the part when compared to the case of 20 droplets related to the size of the 300 µm × 300 µm part. That difference can be seen in Fig. 4.10 and in Fig. 4.11.

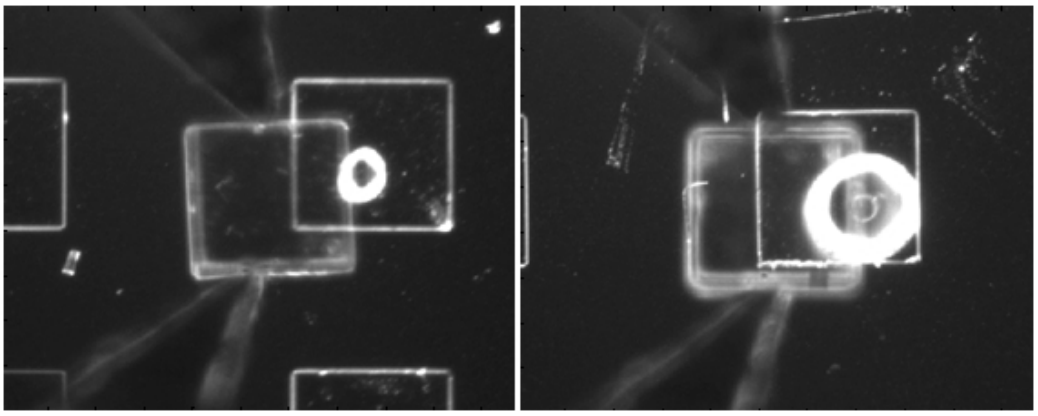

Figure 4.10: 300 µm × 300 µm parts, left: one droplet, right: 20 droplets burst.

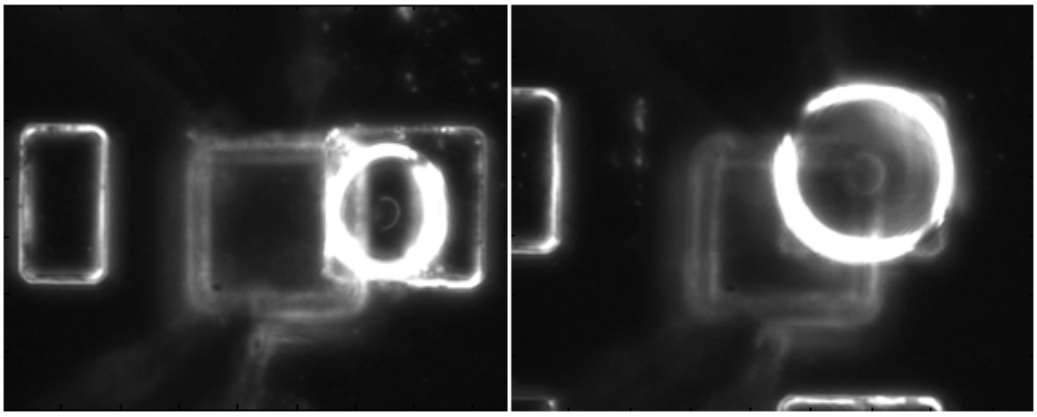

Figure 4.11: 100 µm × 100 µm parts, left: one droplet, right: 4 droplets burst.

4.5.2 Biases

The bias is the difference between the release position and the final position. The biases in x-, y- and z-directions are varied. The tested biases are random values drawn from a uniform distribution between two specified limits in each test. The axes of biases are defined in Fig. 4.12. The same biases are used for dispensing the water droplets and releasing the microparts.

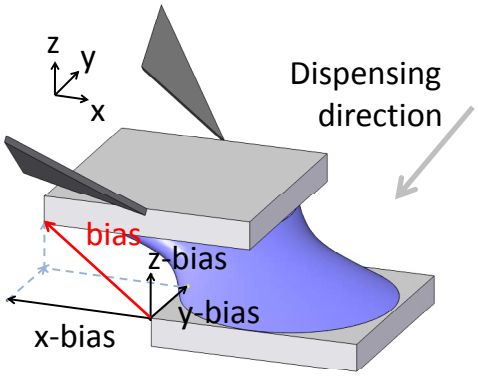

Figure 4.12: The axes of biases.

Before the handling tests with the parts of the same size, the limits of the biases were identified by dispensing 200 times 4 droplets bursts on the top of a 300 µm × 300 µm part and 200 times 1 droplet on the top of a 100 µm × 100 µm part with different biases that spread the area with a random function. The results of those dispensing tests can be seen in Fig. 4.13. The

midpoint of the area where the droplet stays on the top of the part is not in the middle of the part because the dispenser is not perpendicular to the wafer but has an installation angle because of the setup. The dispensing direction is from the top-right corner in the image. The test area for the handling tests was chosen to be a little larger than the area where a droplet can reliably stay on the top of a part.

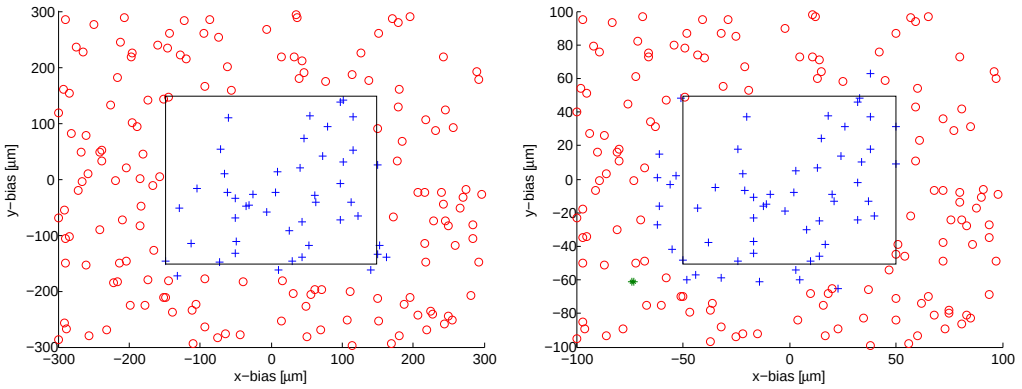

(a) 4 droplets burst on large part

(b) 1 droplet on small part

*Figure 4.13: Droplets dispensed on the top of the part, o = droplet did not stay on the top, + = droplet did stay on the top, * = partly both. Bottom part boundaries are drawn in the image.*

For larger parts, the midpoint of the area of success for dispensing is roughly (20, -20) µm. The droplet stayed on the top of the part with x-biases between -149 µm and 162 µm and y-biases between -173 µm and 142 µm. There was one unsuccessful point (150 µm, 91 µm) in this area. Otherwise the area seems to be quite rectangular and a little larger than the part itself. Based on this result two sets of handling tests with specific biases were carried out: the first one uses a symmetric area with x- and y-biases from -150 µm to 150 µm and the second one uses x- and y-biases from -250 µm to 250 µm. The second set of tests was performed, because the results from the first test set were noticed to be insufficient for determining the area of success. Z-bias was chosen to be between 0 µm to 75 µm for both handling test sets.

Based on the results of the dispensing tests the test area for handling small parts was chosen to be symmetric from -75 µm to 75 µm in both x- and y-axis. A relatively small area was chosen, because previous experience had shown that small parts caused problems, for example, in dispensing accuracy,

when the target is small. However, after data-analysis, it was decided that a larger test area was needed, because there were some successful handlings near the borders of the test area. The additional tested area was an x-bias between -100 µm and -75 µm and a y-bias between -75 µm and -100 µm. The z-bias was chosen to be between 0 µm to 45 µm.

For the handling tests using two parts of different sizes, the biases were chosen to be adequate to show the whole success area – parameters were predicted with the help of the results from the test set with 300 µm × 300 µm parts. The x-bias was chosen to be between -180 µm and 150 µm, which is asymmetric because of the geometry of the part. The y-bias is symmetric between -180 µm and 180 µm. The z-bias was chosen to be the same as with the 300 µm × 300 µm parts. Both x- and y-biases were tested to be adequate by dispensing 200 times four droplets bursts on the top of the 300 µm × 600 µm part (see Fig. 4.14). Before these tests, the dispenser was taken out from the chamber for cleaning, so the angle of the dispenser can be slightly different from the angle used in the tests with the parts of the same size.

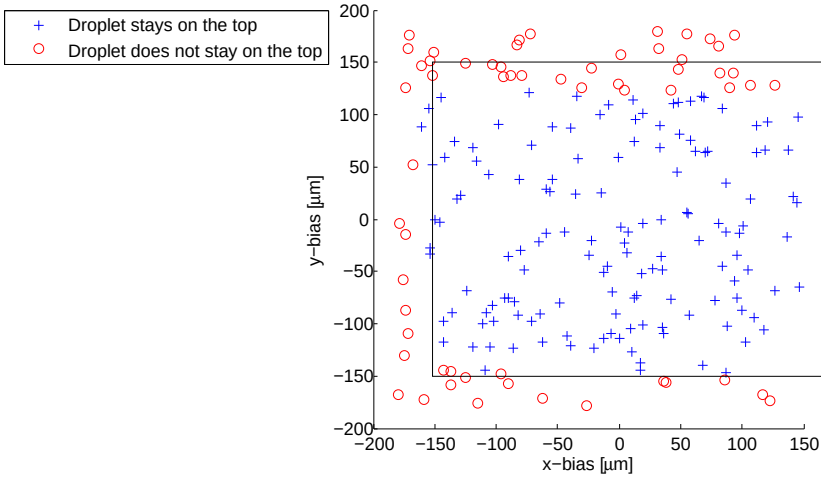

Figure 4.14: 4 droplets bursts dispensed on the top of the 300 µm × 600 part. Bottom part boundaries are drawn in the image.

The dispenser was calibrated every time the bottom part was changed, using the center of the part as a zero position. This, however, was problematic with small parts because the droplet is so large compared to the size of the

part and it was hard to determine the center of the part accurately. That might cause some error to the biases for dispensing.

4.6 Test cycle

In this thesis the basic test cycle of the hybrid assembly method is:

- The top part is picked up with the microgripper
- High speed recording of the handling process is started
- A specific amount of water is dispensed to the desired position with specific biases
- The top part is released with the microgripper above the desired position with specific biases
- The recording is continued for one second after releasing to be able to record the whole alignment
- Recording is stopped and the video file is saved for analysis

The test cycle in more depth can be seen from the flowchart in Fig. 4.15. The test process is partially automated as can be seen from the chart. Some manual phases, however, are still required. Also, the evaluation of the success of the picking phase and the success of the self-assembly are performed by a human operator.

In the beginning of a test set the random bias and droplet number values are uploaded from a file. Automatic picking of a part is possible when the part is aligned well on the top of another and the position (releasing position with zero bias) is saved. In the beginning of the tests, and in the case of unsuccessful self-alignment, the part has to be manually picked and released to reach the correct starting position for the test. Moreover, every time the bottom part is changed the positions for dispensing and releasing have to be redefined and saved.

If the automatic picking is successful, the actual test begins: the positioning stages are driven to the dispensing position to which the biases are added, and then the water is dispensed. The stages are driven to the releasing position to which biases are added and the part is released. The dispensing and the releasing processes are recorded. If the test was not the final one, the test number is increased and the part is picked up either automatically or manually depending on whether the self-alignment was successful of not. After that a new test is performed with new biases and a new number of droplets.

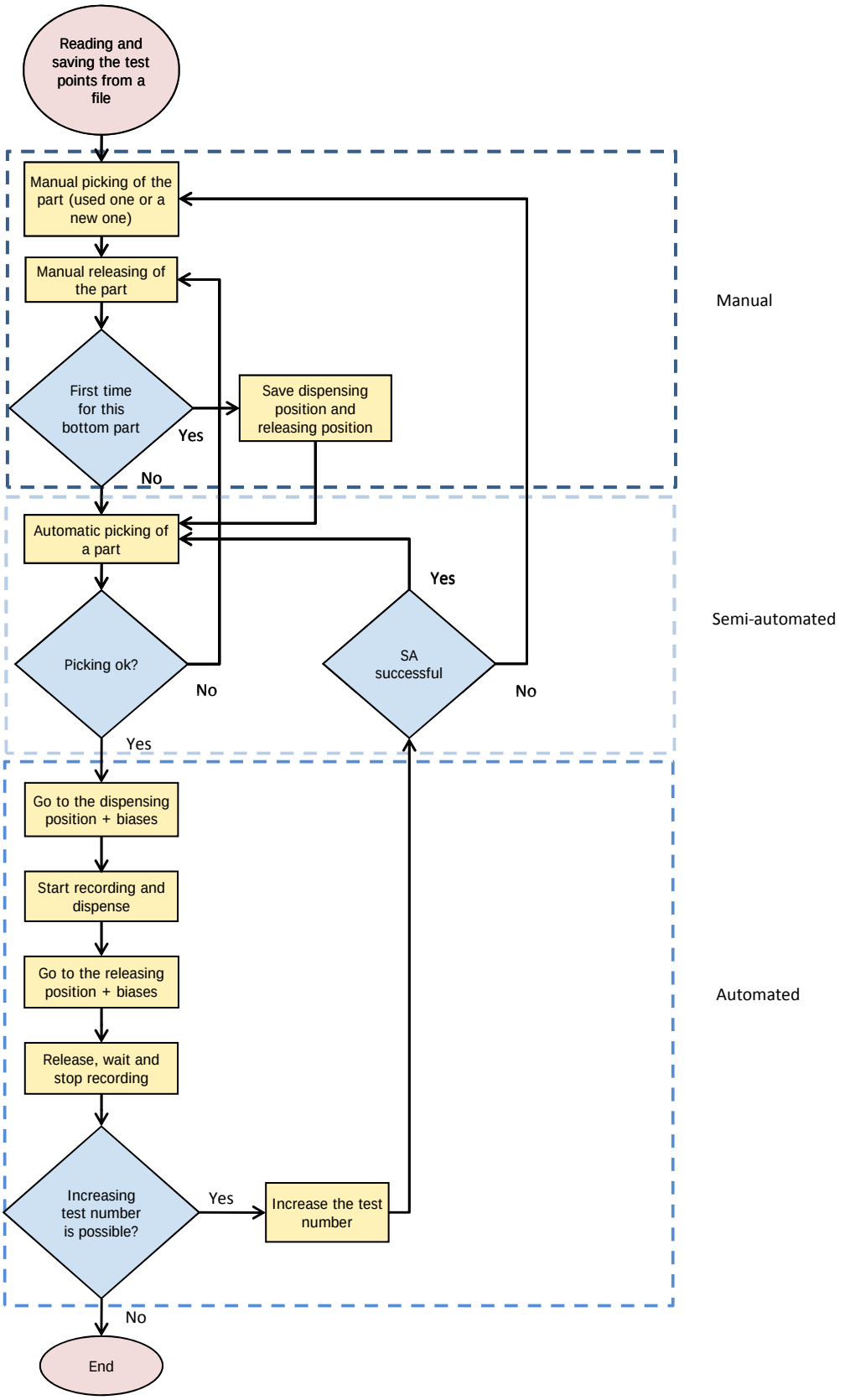

Figure 4.15: The test cycle of hybrid assembly method used in this thesis.

Chapter 5

Experimental Results

5.1 Overview of the tests

The results of three sets of tests that were performed to reach the objectives defined in Section 4.3 are presented in this chapter:

- Assembly of a 300 μm × 300 μm part on the top of another 300 μm × 300 μm part
- Assembly of a 100 μm × 100 μm part on the top of another 100 μm × 100 μm part
- Assembly of a 300 μm × 300 μm part on the short edge of a 300 μm × 600 μm part

The effects of the parameters (see Section 4.5) are carefully analyzed. One method is to define *an area of success* from each test set. That is an area containing all the tests with successful alignment. Changes in the size and shape of the area of success as a function of different parameters are analyzed.

Additionally, *a success rate*, the ratio between successful and unsuccessful tests in some specific area or as a function of different parameters, is used as a tool in the analysis.

5.2 Tests with 300 × 300 micrometer parts

Two sets of handling tests with 300 µm × 300 µm microparts were performed. At first, a symmetric releasing area from -150 µm to 150 µm with different amounts of water and with different releasing heights was tested. Afterwards the test area was noticed to be inadequate to define the limits of the area of success and a second set of tests was performed with a new area from -250 µm to 250 µm. The z-bias was chosen to be between 0 µm to 75 µm and 1-20 droplets were tested.

In total 352 tests were carried out. The combination of two test sets is referred to as *the whole test data* in the analysis. If only the results from the small area – the symmetric area from -150 µm to 150 µm – is analyzed, it is referred as *the data from the small test area*.

5.2.1 Effects of x- and y-biases

Fig. 5.1 shows a scatter diagram of the whole test data plotted against the x- and y-biases. The success rate of the 100 µm × 100 µm segments is visualized by the color of the background. The diagram shows that the success is not possible when the droplet is not on the top of the part. In those cases, a meniscus might not be formed, because the zero level of the z-bias is defined to be on the surface of the bottom part. When a droplet is outside the part, the height of the droplet may be so low that the top part cannot touch the droplet. Even if the meniscus is formed with large positive and negative x- and y-biases, the self-alignment usually fails and the reason for that is natural – the droplet is not on the top of the bottom part.

The dispenser is not installed perpendicular to the wafer and it dispenses at an angle of about 70 degrees to the wafer, causing a small error in dispensing. But in principle, when the droplet is dispensed to the releasing position of the top part, the area of success in handling has roughly the same shape and size as the bottom part. One example of a successful handling can be seen in Fig. 5.2. There are unsuccessful tests inside the area of success, but they seem to be quite uniformly distributed, without coupling between the x- and y-bias. The likely reasons for unsuccessful tests inside the area of success

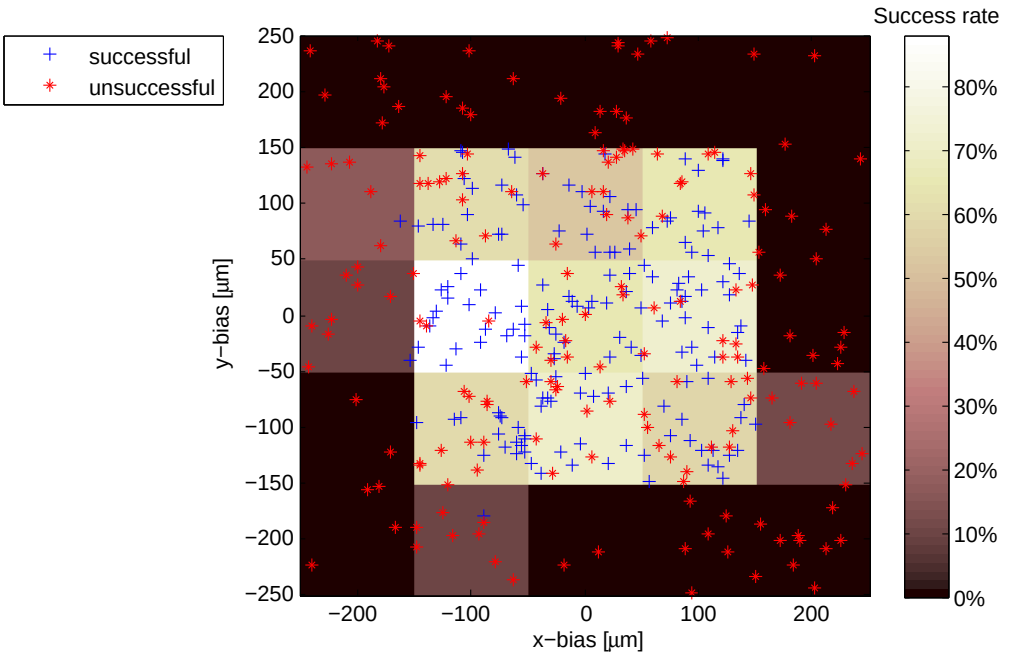

Figure 5.1: XY-scatter diagram of the whole test data. The success rate is shown by the color of each segments background. One segment is 100 µm × 100 µm.

are discussed further in the context of the amount of water and the z-bias in Section 5.2.2.

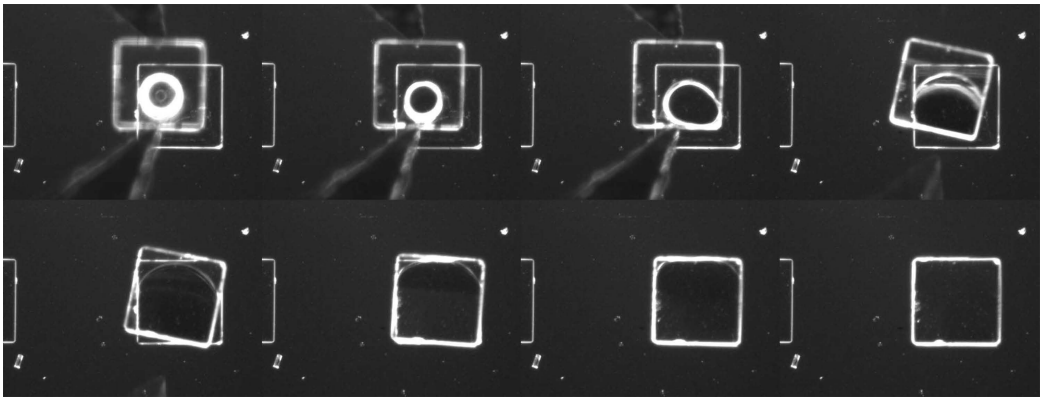

Figure 5.2: An example of a successful handling: X-bias -73 µm, y-bias 73 µm, z-bias 48 µm, 7 droplets.

The same effect of the bottom part boundaries can be observed from Fig. 5.3 where there is an abrupt drop in the success rate as a function of x-bias and y-bias near the edges of the bottom part.

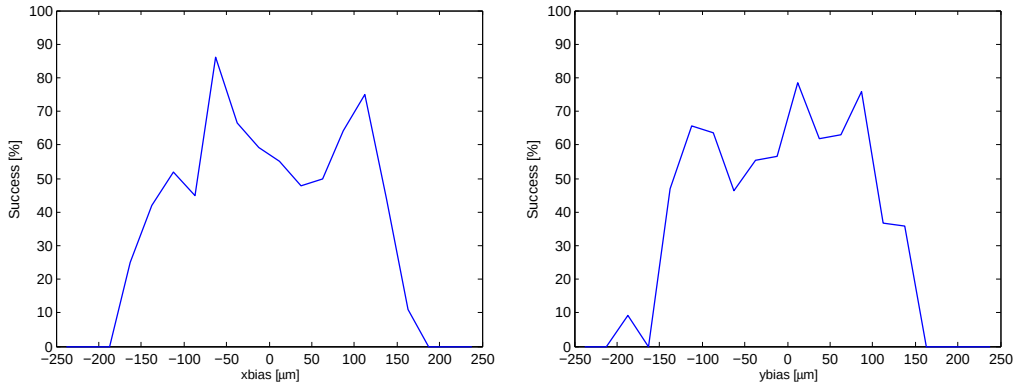

(a) Success rate vs. x-bias

(b) Success rate vs. y-bias

Figure 5.3: Success rates vs. x-bias and y-bias for the whole test data.

A large difference in the area of success is observed when these results are compared to the previous results obtained from the tests where the droplet was every time dispensed to the midpoint of the bottom part (Sariola et al., 2008b): successful self-alignments were observed quite reliably even when the x- and y- biases in releasing approached 250 µm and successful assembly was seen even with a bias of 300 µm in the x- and y-directions. Therefore, the landing position of the droplet has a significant role in determining the area of success.

5.2.2 Effects of z-bias and the number of droplets

It is hard to analyze the effects of the amount of water without taking the releasing height into account or vice versa. This is because of the coupling between the amount of water and the releasing height.

Fig. 5.4 shows a scatter diagram of success/failure against the z-bias and the number of droplets from the data from the small test area. When only the small test area is considered, the coupling effect between the z-bias and the number of droplets can be clearly seen. This is because there are only a few failures caused by large x- and y-biases which are mostly independent from

z-bias and the number of droplets. The z-bias and the number of droplets are coupled – when the number of droplets increases, successful handlings need more space between the parts.

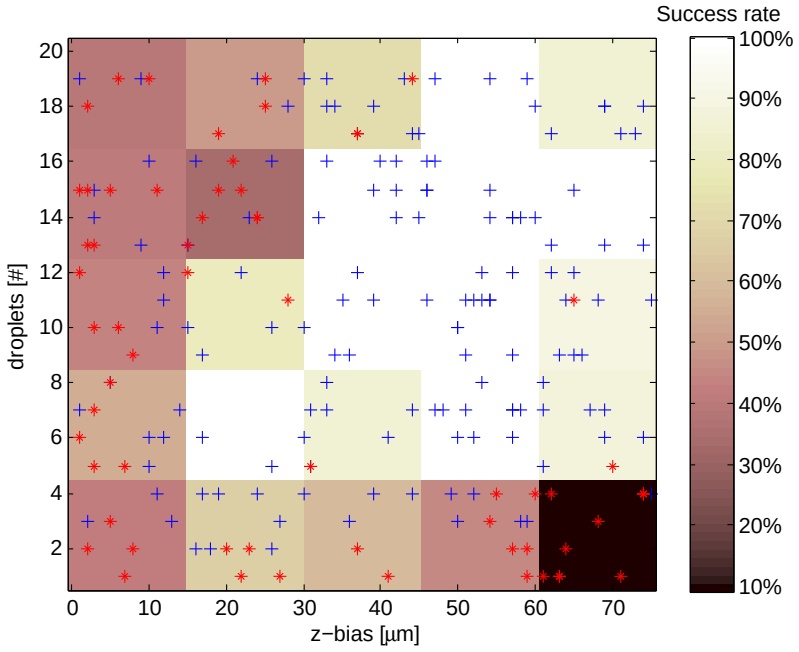

Figure 5.4: Z-bias-droplet scatter diagram for the data from the small test area. The success rate is shown by the background color of each segment. Each segment is corresponding to 15 µm × 4 droplets.

However, not all handlings with a large number of droplets and a small z-bias are unsuccessful, which is due to the direction in which the water flows during the approaching operation when the releasing height is low. If the droplet escapes from the gap between the parts, the self-alignment fails; if it stays on the top of bottom part, there is a chance to succeed.

The totally unsuccessful area corresponds to the parameters set with four or less droplets and a z-bias between 60 and 75 µm. In such cases, the meniscus is not formed because if droplet height is smaller than the releasing height the part will not even touch the droplet. Moreover, the handlings with one or two droplets are usually unsuccessful regardless of the z-bias. With a small releasing height the droplet does touch the top part, but the reason for unsuccessful assembly could be the dry contact because of the small amount of water.

Even though Fig. 5.4 is clear, it hides the effect of the amount of droplets and z-bias on the area of success. The same can be better analyzed when the x- and y-biases are taken into account. Fig. 5.5 shows the whole test data, the same data as in Fig. 5.1 but divided according to the number of droplets and z-bias. Several scatter diagrams of success/failure against x- and y-biases with different combinations of releasing height (z-bias) and number of droplets are shown.

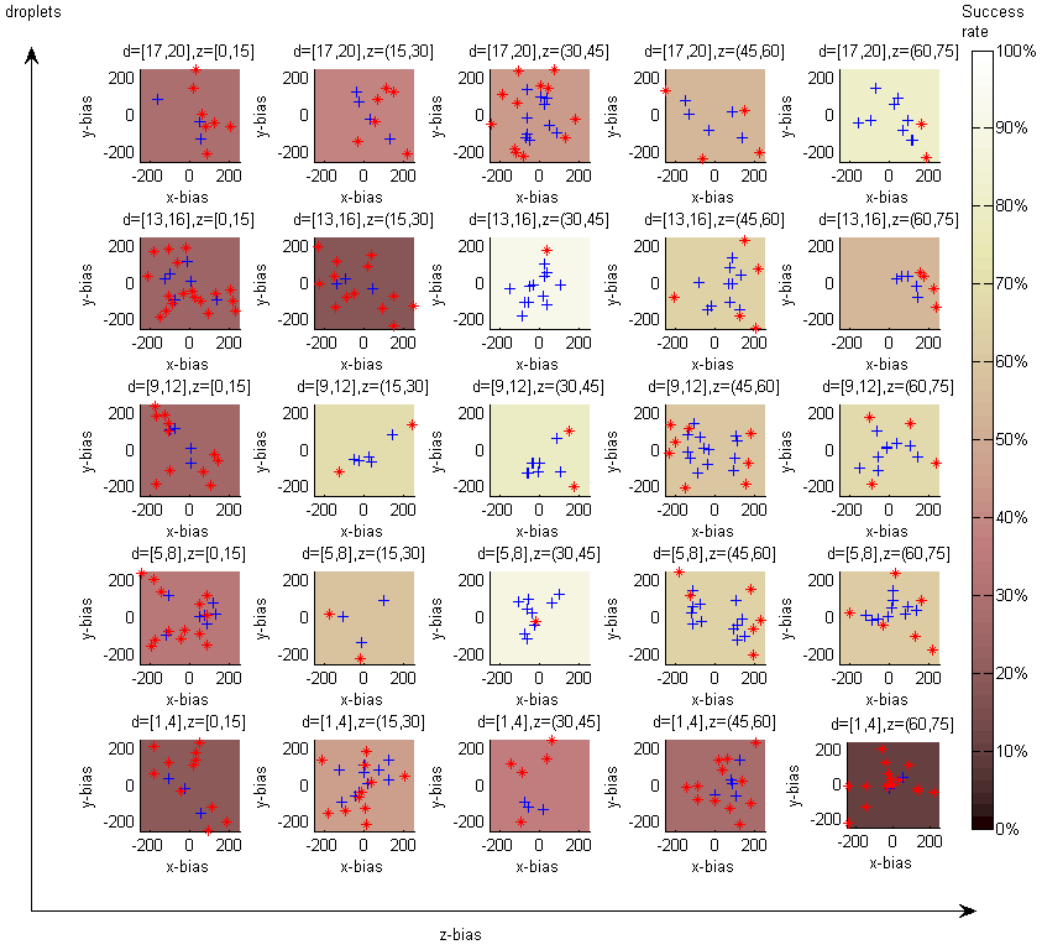

Figure 5.5: Scatter diagram showing the effect of z-bias and the number of droplets for the whole test data.

When Fig. 5.5 is analyzed, some conclusions can be drawn. Some of these were already discussed in the context of Fig. 5.4, but are now confirmed, when the effect of x- and y-biases are also taken into account. The main results are first listed and then discussed:

1. Assembly is unreliable with 1-4 droplets (approximately 170 nl - 680 nl water)
2. Too low releasing height makes the failure more probable
3. The success rate as a function of number of droplets and the releasing height is coupled
4. Assembly is reliable with 9-12 droplets (approximately 1530 nl - 2040 nl water) regardless of z-bias
5. Assembly is quite reliable with z-biases between 30 and 45 µm regardless of the number of droplets

Analysis behind the results:

1. With 1-4 droplets the success rate of the handling is low. There are many failures even when the x- and y-biases are not outside the bottom part. Even though there are some successful handlings it can be concluded that 1-4 droplets are insufficient for reliable handling. In these cases, the meniscus may not be formed because the droplet is so small (that depends on the z-bias – if the droplet height is smaller than the releasing height, there is no contact at all between the droplet and the part) or even if the meniscus is formed there might be a dry contact between the parts, possibly hindering the self-assembly.
2. When the z-bias is small there are more failures. With z-biases between 0 and 15 µm there are failures also in the middle of the area of success. The reason for that might be that when the releasing height is small, water flows easily away from under the part during the approaching operation. However, for the self-alignment process the direction of that flow is critical. If the water escapes from between the parts, self-alignment fails and if the water stays on the top of the bottom part, there is still a chance to succeed. As an example of the effects of low releasing height, 7/10 of the failures in the area of success with 5-8 droplets have a z-bias between 0 and 15 µm.
3. The number of droplets and the releasing height are coupled. 16/17 of the failures in the area of success of the tests with 13-16 and 17-20

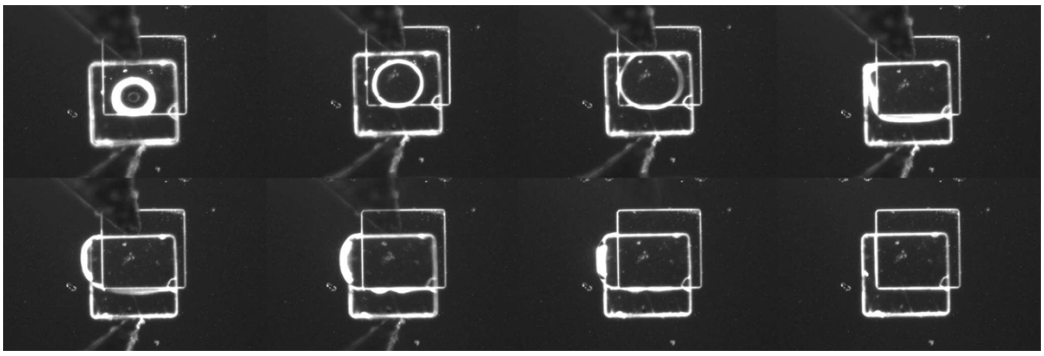

Figure 5.6: Small z-bias: water flows away from between the parts. Releasing height 1 µm (x-bias:-142µm, y-bias:-110µm, 7 droplets).

droplets are due to a releasing height which is too low – they do have a z-bias between 0 and 30 µm. There are now more failures with z-biases from 15-30 µm than with the cases of less droplets: when the amount of water is larger, more space is needed in between the parts for successful handling to prevent the water from flowing away from the gap between the parts. Moreover, even though the tests with the largest z-biases seem to be quite reliable, the combination with the smallest amount of water (1-4 droplets) leads to failures. The part must not be released too high compared to the height of the droplet.

4. When Fig. 5.5 is analyzed row by row, it can be noticed that in the case of 9-12 droplets there are no failures in the area of success; the effect of the z-bias seems to be almost nonexistent. Fig. 5.7(a) shows all the test results with 9-12 droplets regardless of z-biases. The area of success is quite rectangular, making it clear that if the amount of water is chosen well, the handling is less vulnerable to the small changes in other parameters. The failures near the edges of the area of success are probably due to a small z-bias combined to the near-the-edge effect. 7/9 of those failures have a releasing height smaller than 30 µm. Near the edge the water flows easily away from between the parts when the part is released low.

5. When Fig. 5.5 is analyzed column by column it can be seen that with z-biases between 30 and 45 µm there are less failures in the area of success as there are with other segments of z-biases. Also, a segment between 45 and 60 µm gives similar results. The test results with biases

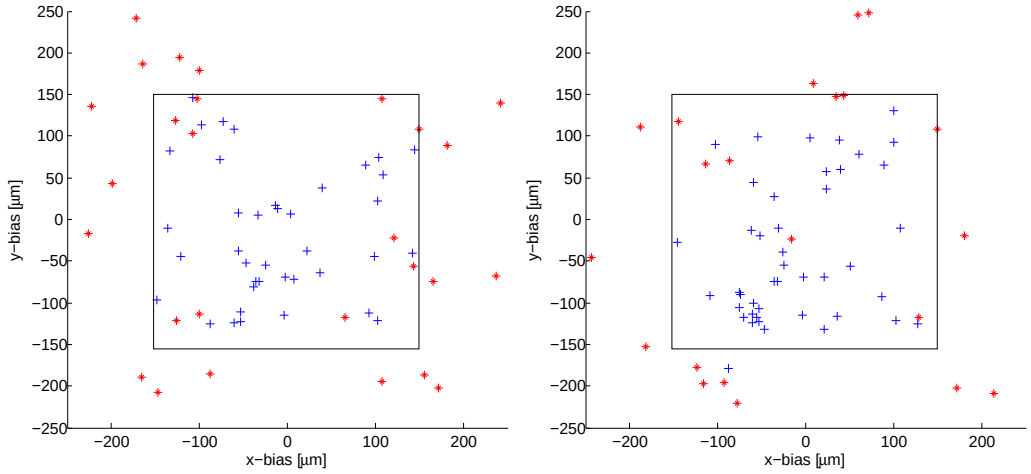

(a) Droplets 9 – 12

(b) Z-bias 30 – 44 µm

Figure 5.7: When the number of droplets or z-bias are chosen well the area of success is quite similar to the area of bottom part – the assembly is less vulnerable to changes in other parameters.

between 30-45 with all amounts of water are in Fig. 5.7(b). When the releasing height is chosen well, the effect of all other parameters is smaller. However, the effect of small number of droplets cannot be totally compensated for by the selection of z-bias: one unsuccessful handling in the middle of 5.7(b) is done with only 5 droplets, which seems not to be enough in all cases. If the amount of droplets is large enough, the handling is very reliable with the z-biases between 30 and 45 µm and even with z-biases between 45 and 60 µm.

Fig. 5.8 illustrates the success rates as a function of z-bias and the number of droplets for the data from the small test area to minimize the effect of large x- and y-biases outside the bottom part. Even though the number of droplets and the z-bias are coupled, the success rates can be studied separately because the parameters of each test are chosen randomly. However, these success rate curves hide the effect of other parameters and the result is only tentative.

Small z-biases have lower success rates and there is a peak in the success rate at 50 µm. Otherwise there seems not to be any clear trend. The success rate vs. droplets seems to be increasing when the number of droplets increases

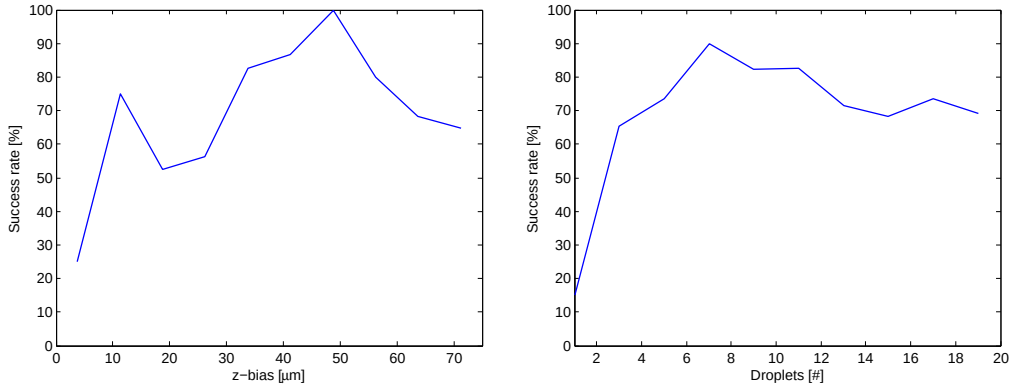

(a) Success rate vs. z-bias (b) Success rate vs. number of droplets

Figure 5.8: Success rates vs. z-bias and number of droplets, only the data from small test area.

until it is 7 droplets. After 7 droplets, the rise ends and the curve turns down or at least is almost constant. The trend in success rate vs. droplets is not as clear as it has been in previous tests when the droplet was dispensed to the center of the bottom part (Sariola et al., 2008b). In those tests the success rate increases constantly when the number of droplets increases. The reason for that difference might be that when the droplets are dispensed near the edge instead of in the middle, the larger droplets may flow over the edge and lead to failures in the handling.

5.2.3 Accuracy

Even though successful and failed tests can be easily distinguished by eye, the accuracy of a successful test cannot be easily identified from optical microscope images. Therefore, the accuracy of hybrid handling was measured using a scanning electron microscope. The results of six successful tests with 300 µm × 300 µm microparts were analyzed.

The side-walls of the parts used in the tests are not perfectly vertical due to the manufacturing process, which causes a size-difference in contacting surfaces. Consequently, it is not possible to measure the accuracy of the alignment directly from one corner. The differences in geometrical centers of both parts and rotation angle are calculated from six SEM-images taken

from two different angles. The method is illustrated in Fig. 5.9. The overview image on the left shows where the closer images are taken from. The image on the right is an example of the images used in the analysis.

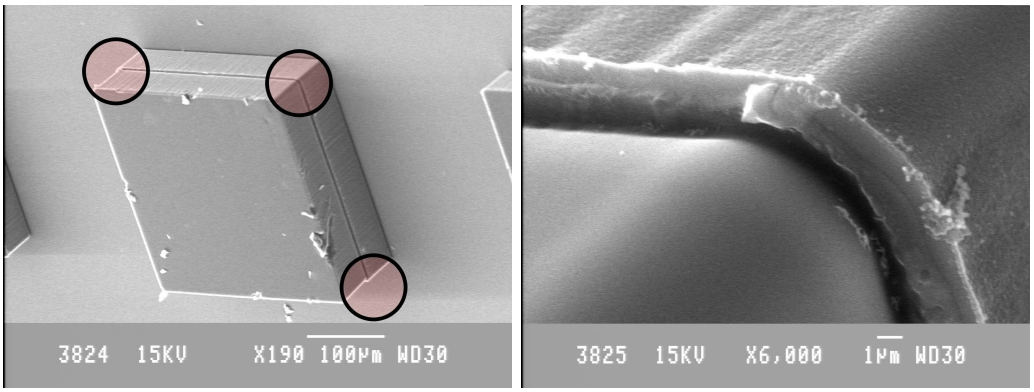

(a) Overview (b) Top-right corner

Figure 5.9: Examples of SEM-images for measuring the accuracy. Overview image shows where closer images are taken from this angle.

The results obtained from the analysis are summarized in Table 5.1. Root Mean Square (RMS) error and Mean Absolute (MA) error are calculated from the results. Assembly accuracies close to the fabrication accuracy of the microparts can be achieved – the fabrication accuracy is about 2 µm. Even though there are some variations in the magnitude of the errors, the differences are small.

Table 5.1: Accuracy of the assembly of 300 µm ×300 µm parts.

Test	x-error [μm]	y-error [μm]	angle-error [°]
1	-0.1	3.1	0.0
2	-0.5	3.3	-0.2
3	-2.6	-0.6	0.2
4	-2.6	1.7	0.0
5	-2.2	-0.8	-1.0
6	-0.6	-1.1	0.0
RMS error	1.8	2.0	0.4
MA error	1.5	1.8	0.2

5.3 Tests with 100 × 100 micrometer parts

Two sets of tests with 100 µm × 100 µm microparts were performed. At first a symmetric releasing area from -75 µm to 75 µm with different amounts of water and with different releasing heights was tested. The size of area, however, was insufficient to determine the area of success, and 40 additional tests were done with an x-bias between -100 and -75 µm and a y-bias between -100 and -75 µm. The z-bias was chosen to be from 0 µm to 45 µm and 1-4 droplets were tested. The data used in the analysis is a combination of these two sets of tests.

5.3.1 Effects of x- and y-biases

From Fig. 5.10 it can be observed that successful handlings are strongly influenced by the x-bias and y-bias. The effects of the bias are not as clear as with the 300 µm × 300 µm parts. When the releasing points inside the area of success are studied, unsuccessful points seem to be rather uniformly distributed while the x-bias and y-bias do not have a noticeable effect.

The center of the area of success is not in the middle of the bottom part, although the dispenser was calibrated by dispensing water to the center of the part. The installation of the dispenser was not moved after the tests with the 300 µm × 300 µm parts, so the same effect should have been noticed with 300 µm × 300 µm parts also. The reason for this shift in the area of success might be the error in calibrating the dispenser: it is more difficult to calibrate the dispenser to dispense droplets to the center of a small part than to the center of a large part – the droplet is so large compared to the size of the part. Another reason is that the droplet is not a point, but is rather spread on a comparably large area to the size of the part. That affects how the droplet is positioned on the part.

The boundaries of the area of success can also be observed from Fig. 5.12 which shows the success rates of the handling as a function of x-bias and y-bias. The boundaries are not as sharp as with the 300 µm × 300 µm parts. It can, however, be concluded that dispensing outside the part will not lead to successful assembly even though with these smaller microparts the dispensing

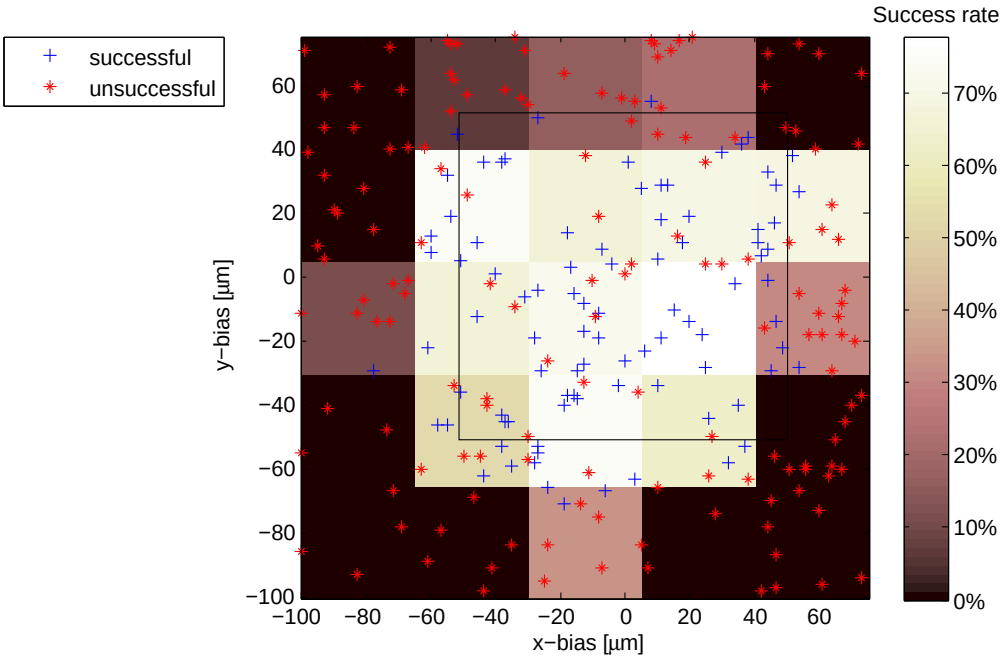

Figure 5.10: XY-scatter diagram of the tests, success rate is shown by the background color of each segments. One segment is 35 µm × 35 µm. Bottom part boundaries are drawn in the image as a black rectangle.

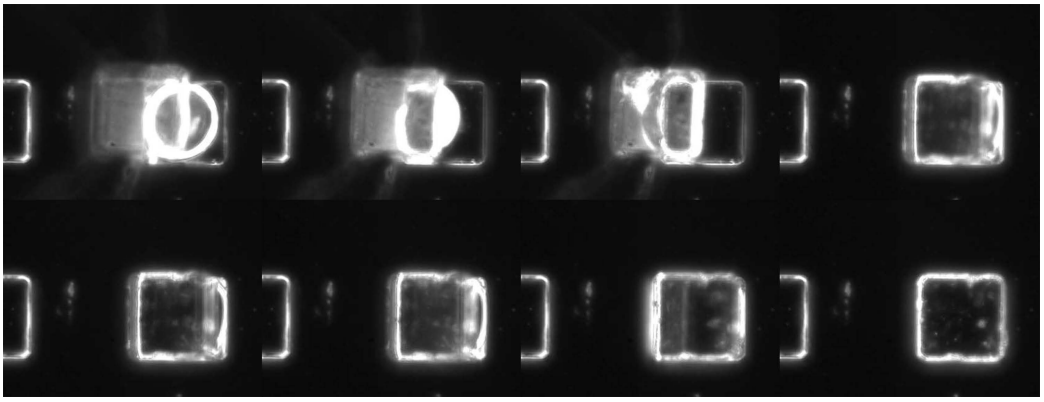

Figure 5.11: An example of a successful handling with large x-bias: X-bias -60 µm, y-bias 8 µm, z-bias 41 µm, 2 droplets.

accuracy compared to the part size is so poor that some droplets that were meant to be outside the part were actually on top of it.

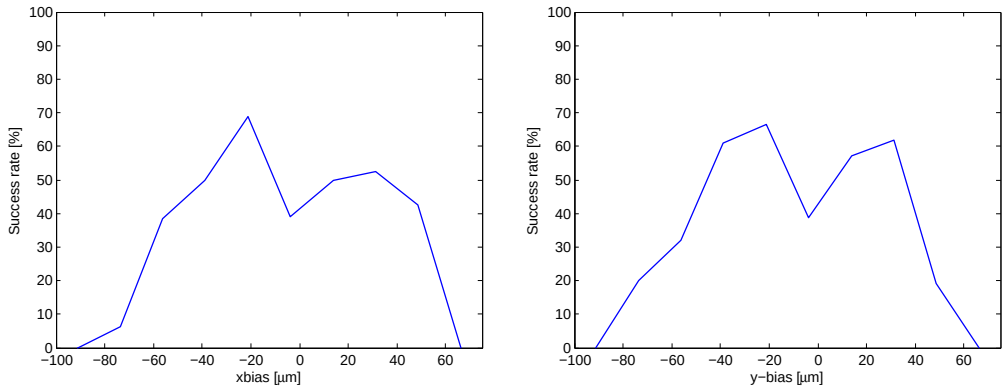

(a) Success rate vs. x-bias

(b) Success rate vs. y-bias

Figure 5.12: Success rates vs. x-bias and y-bias.

5.3.2 Effects of z-bias and the number of droplets

For the analysis of the effects of the z-bias and the number of droplets, the data in Fig. 5.10 is divided in Fig. 5.13 according to the number of droplets and z-bias. Scatter diagrams showing the success/failure against the x- and y-biases with different combinations of z-bias and number of droplets are presented.

The main results are listed below followed by a discussion:

1. Already one droplet is enough for successful assembly
2. A small z-bias (< 9 µm) makes the handling slightly unreliable
3. A large z-bias (> 36 µm) is problematic with one droplet, otherwise z-biases 10 - 36 µm have no effect on reliability
4. Coupling between the z-bias and the number of droplets is not as clear as with 300 µm × 300 µm parts

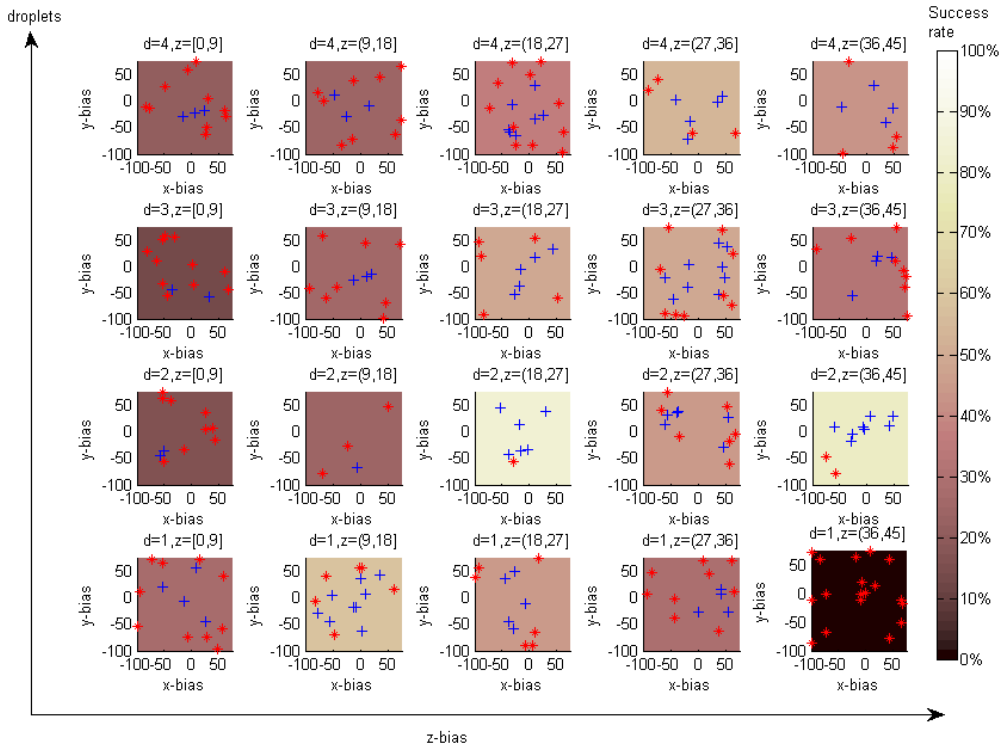

Figure 5.13: Scatter diagram showing the effect of z-bias and the number of droplets.

1. Fig. 5.13 shows that one droplet is already enough for successful handling for 100 µm × 100 µm microparts. One droplet contains so much water that it is able to wet the whole surface. No dry contact can happen to prevent the self-assembly. The only limiting factor for dispensing one droplet seems to be the releasing height – if the part is released too high (36-45 µm), the meniscus is not formed at all. Lower releasing height seems to have no problems with one droplet.

2. The effects of the z-bias can be seen in Fig. 5.13. When the z-bias is smaller than 9 µm, failures are quite uniformly distributed and more probable than with z-biases larger than 9 µm. With only one droplet, the reliability is good also when released low but with two droplets most of the failures have a low releasing height, which may be the reason for unsuccessful assembly. In the cases when the numbers of droplet are 3 and 4, the result seems to be quite identical. Unsuccessful results in the area of success (there are only a few) all have a releasing height lower than 9 µm. Similarly to the 300 µm × 300 µm parts tests, water

flows away from the gap between the parts and the direction of the flow is critical for self-assembly.

3. As discussed previously in the context of the first result, there are problems in the assembly when the releasing height is more than 36 µm. There are a group of failures in the area of success with one droplet – the height is too high for meniscus forming. When the amount of water is larger, the height over 36 µm no longer has that negative effect. For the releasing heights of 10 - 36 µm, the areas of success are quite symmetric, and there are only a few disjointed unsuccessful handlings.

4. A clear trend that has been noticed for the 300 µm × 300 µm parts – when the number of droplets increases, a successful handling needs more space between the parts – is not as clear with the small parts even though some clue can still be seen from Fig. 5.13. The reason might be that the droplet size is so big compared to the size of the part that other more random reasons of failure are predominant. For example, a larger droplet can flow easily over the edge and a number of 2 to 4 droplets will have a similar chance for such phenomenon to occur which results in a similar success rate for all droplet sizes.

Fig. 5.14 presents the success rates as a function of z-bias and the number of droplets. In Fig. 5.14(a) with the z-bias, the curve has a peak – too small and too large biases might cause failures. However, this trend is not very clear. Fig. 5.14(b) shows that the number of droplets seems not to have a strong effect on success rate. Four droplets are not yet on the limitation where water would overflow and one droplet is enough to prevent the dry contact between the parts. Yet two droplets seem to be the optimum.

5.3.3 Accuracy

The accuracy of the assembly was measured in a way similar to the larger microparts from the five successful tests using the SEM. The size difference of the contact areas can be clearly observed in Fig. 5.15. Therefore, the geometrical centers of the parts are calculated instead of measuring only the mismatch corner. The method to obtain the x- and y-error and angle error

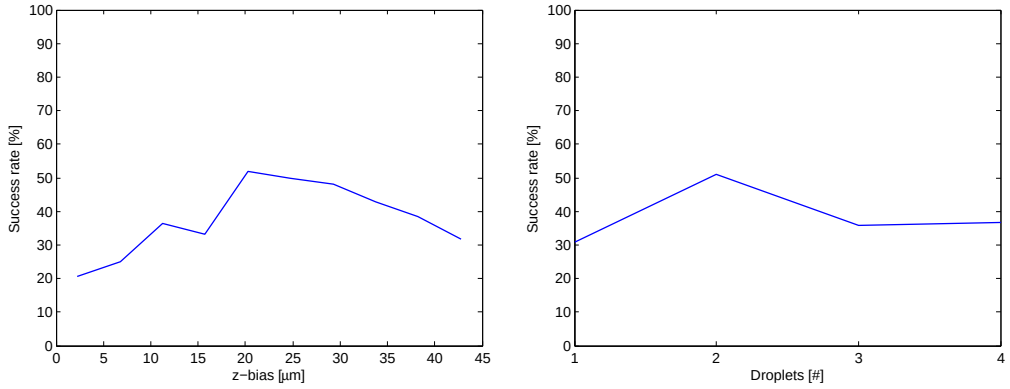

(a) Success rate vs. z-bias (b) Success rate vs. number of droplets

Figure 5.14: Success rates vs. z-bias and the number of droplets.

is the same as in previous tests (see Section 5.2.3). The calculated values are shown in Table 5.2 – the assembly accuracies are close to the fabrication accuracy (2 µm) similar to the assembly accuracy of the 300 µm × 300 µm parts.

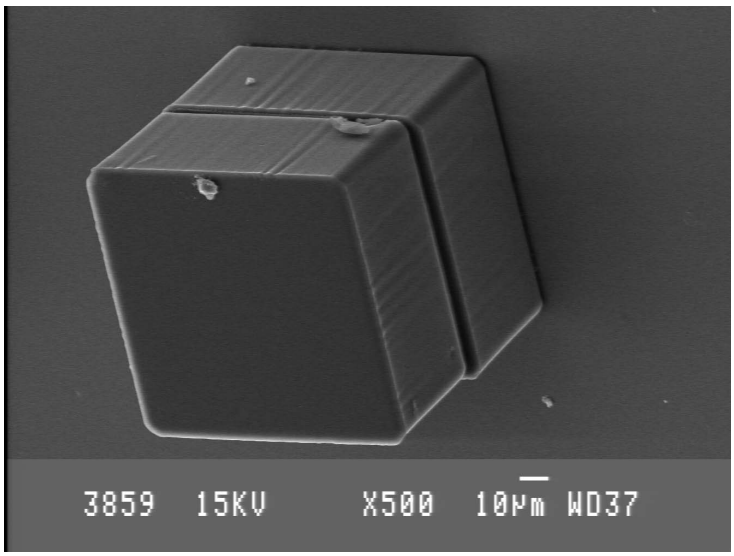

Figure 5.15: SEM image shows that the contact areas have different sizes due to non perfectly vertical walls.

Table 5.2: Accuracy of the assembly of 100 μm ×100 μm parts.

Test	x-error [μm]	y-error [μm]	angle-error [°]
1	2.1	2.4	0.4
2	2.1	-0.6	-0.4
3	0.2	2.1	0.0
4	-2.1	0.1	-0.4
5	-2.4	-3.7	-0.5
RMS error	1.9	2.2	0.4
MA error	1.8	1.8	0.4

5.4 Tests with parts of different sizes

A set of handling tests with 300 µm × 300 µm microparts on the top of 300 µm × 600 µm microparts was performed to study the effects of different parameters on hybrid assembly of parts of different sizes. The tested releasing area was: x-bias between -180 µm and 150 µm, y-bias between -180 µm and 180 µm and z-bias between 0 µm and 75 µm. Different numbers (1-20) of droplets were used in the tests as previously with the 300 µm × 300 µm microparts.

5.4.1 Effects of x- and y-biases

Fig. 5.16 shows a scatter diagram of the test results against x- and y-biases. The area of success is quite evident – there are only a few tests with self-alignment when the y-bias is larger than 100 µm or smaller than -130 µm. The area is shifted a little in the direction of dispensing: there are more successful handlings with negative y-biases – the direction of dispensing has an effect. The side where the dispenser is, contains less successful handlings than the others.

The borderline between successful and partially successful tests seems to be slightly over zero in the x-axis. When the x-bias is negative, the final position of a successful handling is in the short edge of the bottom part (see Fig. 5.17). There are some individual successful handlings also with larger

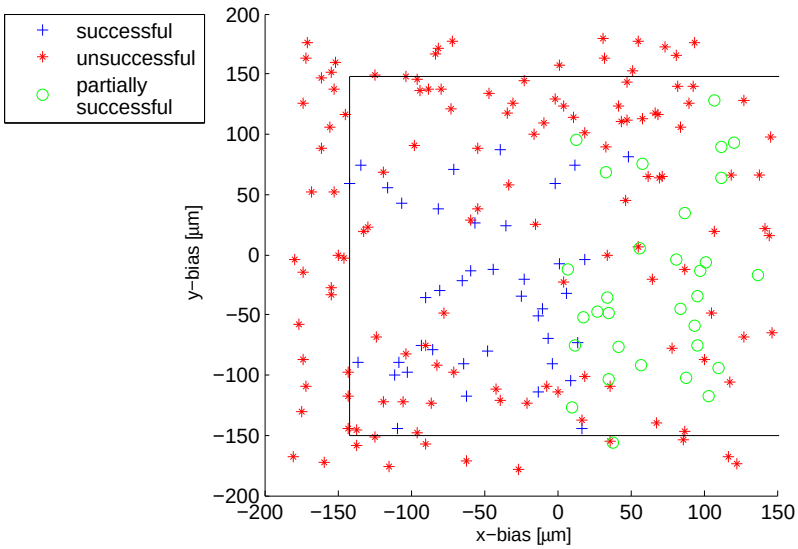

Figure 5.16: Scatter diagram of the assembly of a small part on the top of a large part. Boundaries of the bottom part are drawn in the image.

positive biases. Even small positive x-biases may prevent successful handling and cause partially successful or unsuccessful handlings. The best success rate is with small negative x-biases combined with small y-biases.

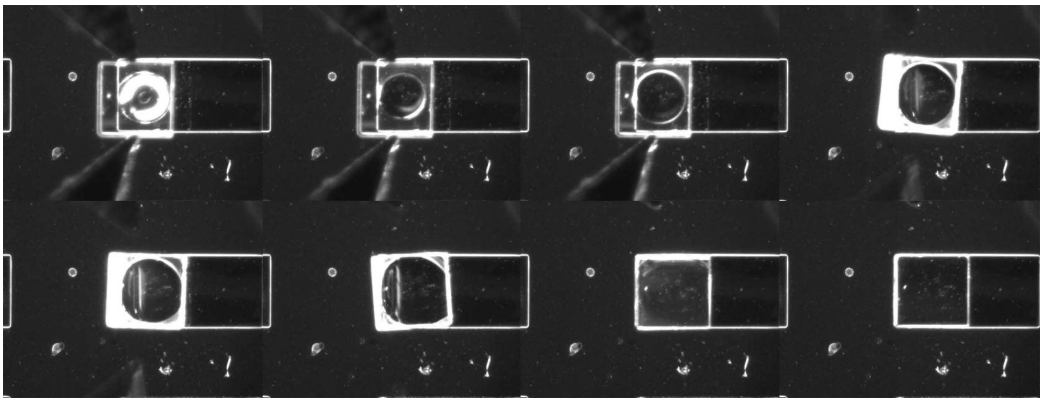

Figure 5.17: When x-bias is negative, the top part aligns to the short edge of the bottom part when the assembly is successful. X-bias -80 µm, y-bias -30 µm, z-bias 66 µm, 18 droplets.

Fig. 5.18(a) illustrates more of the effect of the size-difference. The success rate vs. x-bias is calculated from the successful tests only, that is the tests where the final position is in the short edge of the bottom part. It can be clearly seen that when the x-bias is positive, there is an abrupt drop in

success rate. There are still some successful tests with an x-bias over that limit: the possible reason is that if the water flows in the direction of the short edge it may reach the edges and a meniscus is formed in the desired position. When the distance is too long, however, that is not possible.

The effect of the dispenser can be seen also in Fig. 5.18(b). The success rate vs. y-bias includes also partially successful tests – it is actually a success rate of self-alignment, not a success rate of desired alignment on the short edge. With large positive y-biases, the success rate is lower than with large negative biases. Dispensing is done from the positive y-bias direction, more precisely from the upper right corner of Fig. 5.1.

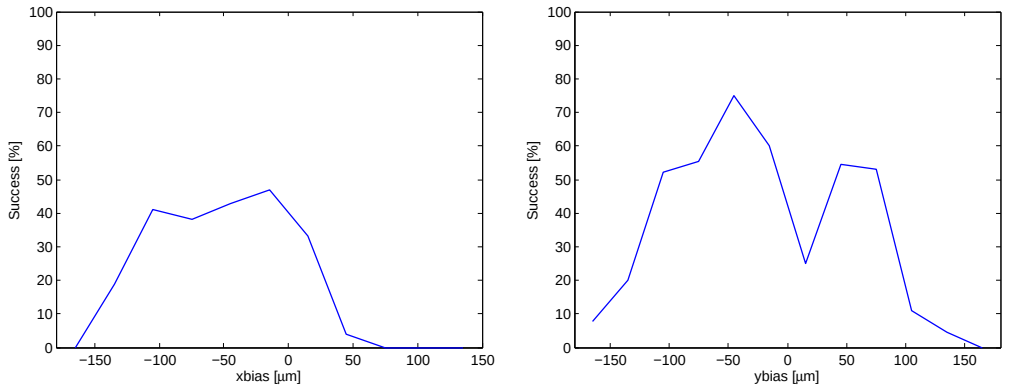

(a) Success rate vs. x-bias

(b) Success rate vs. y-bias

Figure 5.18: Success rates vs. x-bias (only successful tests) and vs. y-bias (also partially successful tests are included).

5.4.2 Effects of z-bias and the number of droplets

Fig. 5.19 contains the same data as Fig. 5.16, but the data is divided according to the number of droplets and z-bias. Several scatter diagrams against x- and y-biases with different combinations of the releasing height (z-bias) and the number of droplets are shown. The background color shows the success rate, where partially successful tests are also included in the success rate.

The distribution of the test points is problematic: there are many combinations of the number of droplets and z-bias with which the number of test

points is too low or there are large areas without any test points. That is because of the randomness in the nature of the selection process of the points.

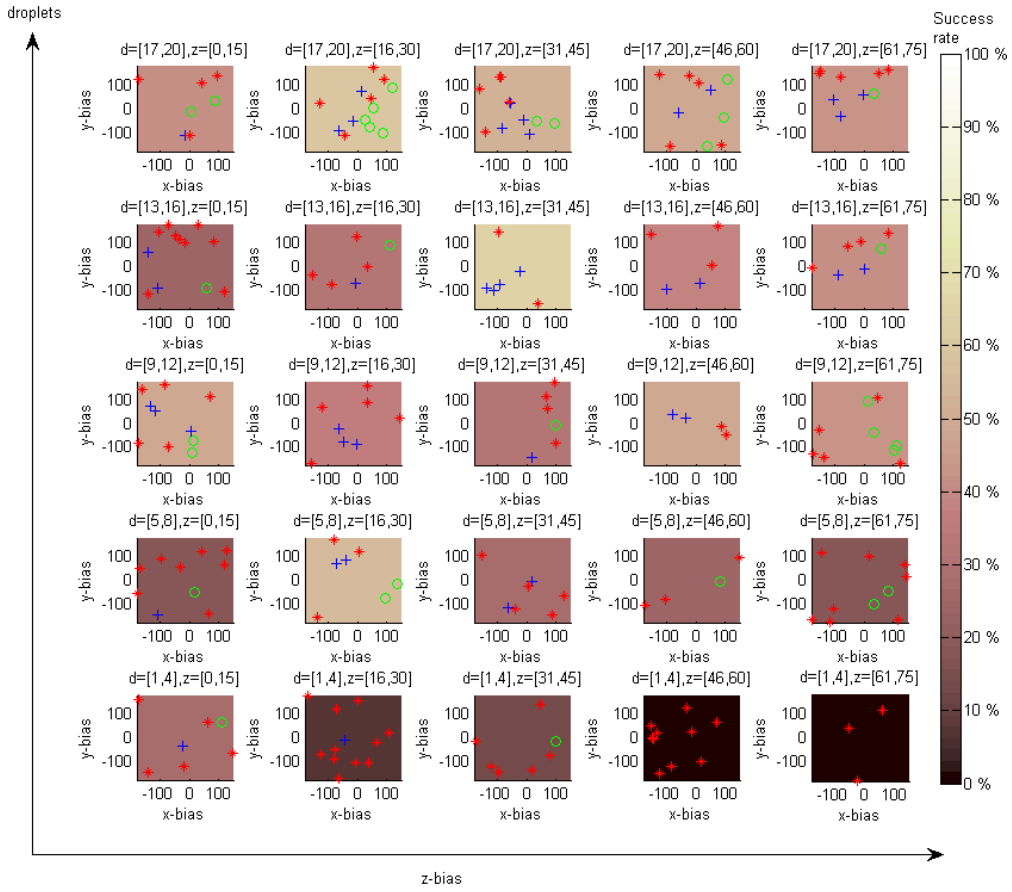

Figure 5.19: Scatter diagram showing the effect of z-bias and number of droplets.

The main results are firstly listed and then discussed:

1. Assembly is unreliable with 1-4 droplets
2. Too low or too high releasing distance may cause problems in assembly
3. Geometric configuration makes the success rate lower
4. Surface impurities seem to affect more the assembly result than in the assembly of the microparts of the same size
5. Coupling between the number of droplets and z-bias is not as clear as with the 300 µm × 300 µm parts

The analysis behind the results:

1. Similarly to the results with the 300 µm × 300 µm parts, the assembly is unreliable with 1-4 droplets. For the cases of 1-4 droplets, there are only a few successful handlings and three of those successful points have a z-bias of 26 µm or smaller. With a small amount of water, the low releasing distance makes successful assembly more probable but still unreliable.

2. The analysis of the effects of the z-bias is hard, due to a relatively low amount of tests per analyzed segment. However, some failures are certainly due to too high or low releasing position. For example, when the number of droplets is in the range of 5 to 8 and the releasing height is larger than 60 µm, the top part does not always touch the droplet before releasing and the formation of the meniscus is failed. In some tests with a low releasing distance, the water flows away from the gap between the parts, leading to a dry contact between the parts. However, low or high releasing positions do not always lead to failures; there is a successful handling with releasing height of 1 µm and also one partially successful with releasing height of 67 µm in this droplet number segment.

   With the largest number of droplets tested (from 17 to 20 droplets), the success rate seems to be the best (see the top row of Fig. 5.19). The main reason for the failures in that segment seems to be the low releasing position. When the droplet is large, more space is needed between the parts. All failures in the area of success are caused by the water flowing over the edge because of the small z-bias.

3. For parts of different sizes, one special problem is due to the fact that the bottom part is larger than the top part. The position of the inner edge of the top part does not contribute to the equation of energy minimization. Moreover, water between the two parts can flow freely towards the open area of the bottom part. In many tests, the top part just seems to stay where it is placed even though the part is wetted thoroughly – the energy minimum is not found and the self-alignment does not happen.

Such an example can be seen in Fig. 5.20: the geometric configuration prevents the self-alignment. The part rotates a little but does not find the energy minimum.

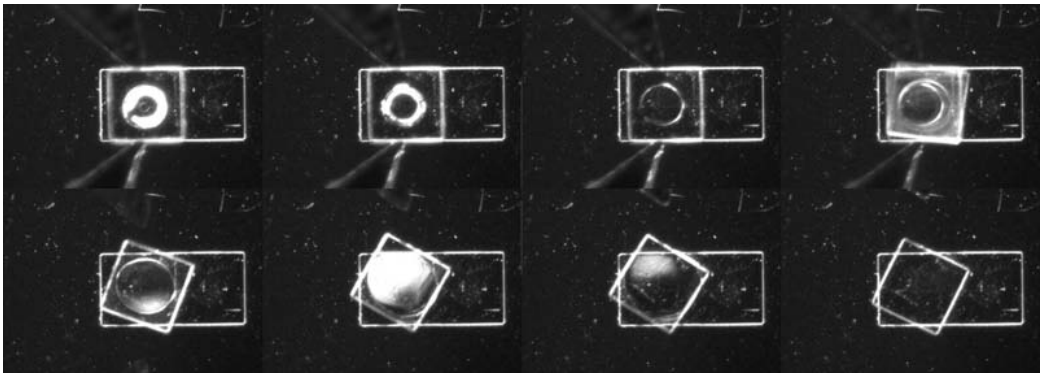

Figure 5.20: An example of the effects of the geometric configuration. X-bias 34 µm, y-bias 0 µm, z-bias 22 µm, 13 droplets.

4. Surface impurities seem to affect more the assembly result than with microparts of the same size. Some of the tests are almost successful and, in some cases, the unsuccessful tests are sequential. If there has been some dust in between the parts in one test it might also affect the next test. Some of the unsuccessful tests that are possibly due to surface impurities rather than parameters of the handling are listed in Table 5.3.

Table 5.3: Examples of unsuccessful tests possibly due to surface impurities.

Test number	x-bias	y-bias	z-bias	droplets
1	33	90	18	10
2	105	-48	57	9
3	-119	68	28	12
4	70	64	38	12
5	55	7	54	13

All the x-bias and y-bias combinations in Table 5.3 are in the area of success, and also the numbers of droplet and z-biases are in the "safe area", not very high or low. Two times among those unsuccessful handlings, there are two sequential tests where the other handling is

almost partially successful (tests 1 & 2 and 3 & 4), which may suggest dust or some impurity between the parts which prevents the final alignment. That may have caused also the next or previous test to fail. The test 5 with an x-bias of 55 μm and a y-bias of 7 μm is almost partially successful, again there might have been some dust causing friction.

With the 300 μm × 300 μm parts of the same size, there were not such almost successful tests (see Fig. 5.21). It is possible that the surface impurities and the friction had a more noticeable effect on the assembly because the energy minimum to drive the self-assembly is not as clear as when the parts have the same dimensions.

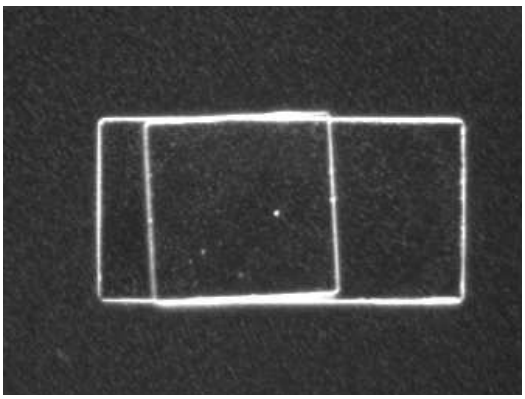

Figure 5.21: Final position of the test 4 in Table 5.3 with possible dust on surface: X-bias 70 μm, y-bias 64 μm, z-bias 38 μm, 12 droplets.

5. Some individual failures were already reported to be due to excessive size of the droplet and low releasing position. However, such effect cannot be seen on the large scale (the effect that a large droplet needs a higher releasing position compared to smaller droplet). The difference in size of the parts causes so many failures that the coupling between the size of the droplet and releasing height is mostly hidden. However, 1-4 droplets combined with too high releasing distance (larger than 45 μm) prevents the assembly, because a meniscus is not formed.

Fig. 5.22(a) shows the success rate as a function of z-bias. Partially successful tests are included in the calculation of the success rate. It appears that the z-bias has no overall influence on the success rate for such tests. If we examine

Fig. 5.22(b), it can be noticed that a larger amount of water leads to better success rate in handling. This may be caused by the fact that the bottom part is larger than the top part: The water can flow freely towards the open area of the bottom part and, with a small amount of water, it is more probable that it does not even reach any of the edges.

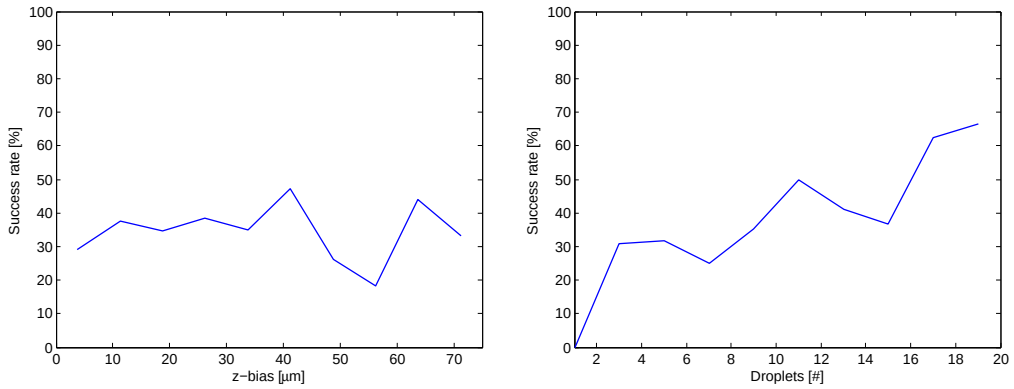

(a) Success rate vs. z-bias

(b) Success rate vs. number of droplets

Figure 5.22: Success rates vs. z-bias and droplets (also partially successful tests are included in both success rates).

5.4.3 Accuracy

The accuracy of the handling tests with parts of different sizes was measured using the same methods as previously (see Section 5.2.3). The results of seven handling tests are analyzed and the results of the analysis are contained in Table 5.4.

The RMS error in the y-direction is larger than that of parts of the same size. The difference is mainly caused by one test with a 7.5 µm error. The resulted assembly of that test is shown in Fig. 5.23. Near the top edge of the bottom part, on the left, there is a small particle, which is suspected to be the reason preventing the final alignment.

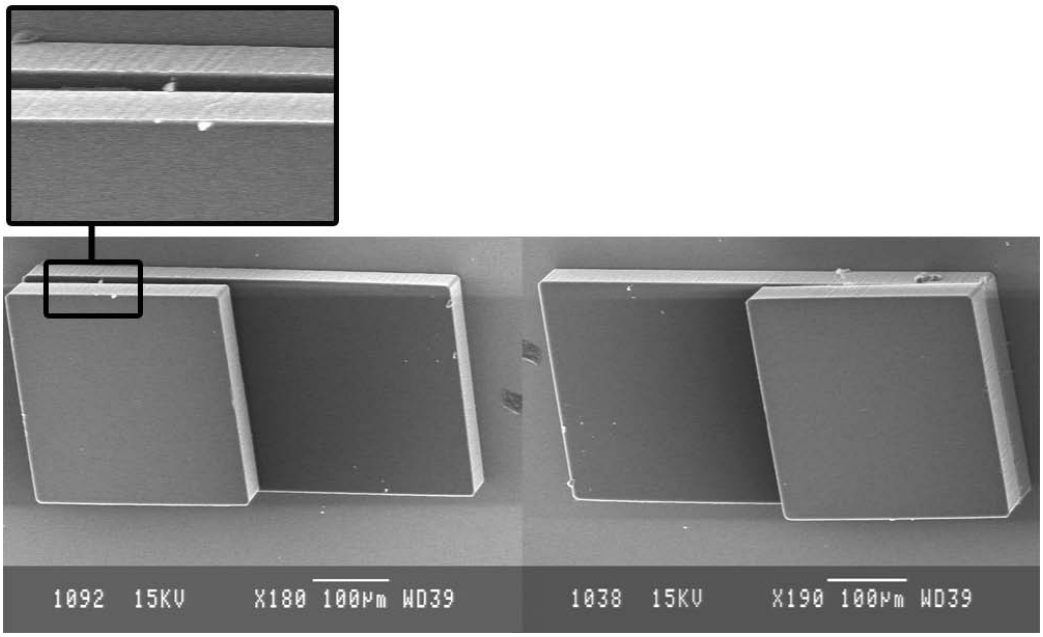

Figure 5.23: The accuracy test with largest error. The images are taken by a SEM from two different angles, a dirt particle is between the two parts.

Table 5.4: Accuracy of the assembly of 300 µm × 300 µm part on 300 µm × 600 µm part.

Test	y-error [μm]	angle-error [°]
1	-2.7	-0.5
2	-0.8	0.6
3	-3.4	0.1
4	0.2	0.1
5	-1.8	0.0
6	0.4	0.2
7	-7.5	0.3
RMS error	3.4	0.3
MA error	2.4	0.3

5.5 Summary and discussion

Clearly, the forming of a meniscus is critical for self-alignment. Many parameters, including the amount of water, the releasing height and biases, all have an effect on the probability of the meniscus forming.

The optimal amount of water to be used in hybrid handling is dependent on the size of the assembled parts. In the case of the 300 µm × 300 µm parts and parts of different sizes (300 µm × 300 µm part on the top of 300 µm × 600 µm part), the experimental results show that 1-4 droplets (170 nl - 680 nl water) are not sufficient for reliable handling. The success rate is not high because of the dry contact between the parts and the difficulties in meniscus formation. However, for the 100 µm × 100 µm parts, one droplet already is enough to wet the whole surface and can lead to successful assembly.

When the releasing height is too low or too high, the unsuccessful handling is quite probable. Low releasing position leads to failures because the water may flow away from the gap between the parts when the top part is pushed downwards. If the direction of the flow is outwards of the edge of the bottom part, the handling is usually unsuccessful. When the part is released at too high a distance, there is the possibility that a meniscus is not formed at all between the parts if there is no contact between the top part and the droplet. If the amount of water is chosen well, the releasing height does not have much effect. This is something, which could be observed in the tests with the 300 µm × 300 µm parts when 9-12 droplets (approximately 1530 nl - 2040 nl water) were used.

A coupling between the amount of water and the releasing height is observed in the tests for both the 300 µm × 300 µm parts and the 100 µm × 100 µm parts. When the number of droplets increases, more space is needed between the parts. The trend is clear with the parts of the same size, but not visible at all for the tests with parts of different sizes – with these parts there were more failures because of the size-difference which obscured the coupling effect.

The area of success has roughly the same size as the bottom part in the case of microparts of the same size. When the droplet lands on the top of the micropart, success is possible. Sometimes the landing position is on the top of

the micropart even though it was meant to be outside, because the droplet is not a point but is spread over a larger area. Moreover, the installation angle of the dispenser has an effect on dispensing accuracy. When the area of the success is compared with the result from the previous tests (Sariola et al., 2008b), the dispensing location has a significant effect on success. When the droplet was dispensed on the center of the bottom part, regardless of the bias in releasing, larger biases lead to success. For example, in the tests with the 300 µm × 300 µm parts, a successful assembly was observed even with a bias of 300 µm in x- and y-directions, while the limit is about 150 µm when the droplet is dispensed to the releasing position of the micropart.

In some individual tests, the reason for failure was a part released near the edge from a quite low releasing height while the droplet dispensed is rather large. A large droplet causes more failures when dispensed near the edges of the bottom part which makes the area of success smaller. When the droplet is small, failures are more uniformly distributed also when the droplet is dispensed near the midpoint of the bottom part. However, the coupling between all parameters (droplet size, releasing height, x- and y-bias) cannot be seen so clearly on the large scale: low and high releasing positions and either too small or large amount of water may cause problems regardless of the x- and y-bias.

For the tests with parts of different sizes (300 µm × 300 µm part on the top of 300 µm × 600 µm part), the top part can align to the short edge of the bottom part if the top part is released near the short edge. If the top part is released with a positive x-bias, the self-alignment may be successful and the final position is in the middle of the bottom part instead of the short edge.

In the tests with parts of different sizes, there are quite many inexplicable failures in the area of success where the alignment does not begin or the final alignment is not achieved. One explanation is the geometric configuration – the inner edge of the top part does not contribute to the equation of energy minimization. Moreover, water between the two parts can flow freely towards the open area of the bottom part. It is also possible that dust or impurities on the bottom part surface have more effect on the assembly of parts of different sizes because the energy minimum is not that deep.

The measured accuracy of the assembly is close to the fabrication accuracy of the microparts in all tests. For the test results using small and large microparts of the same size, the translational accuracy is about 2 μm, but for the tests with parts of different sizes the result is 3.4 μm. The reason for the difference is that one test has a large 7.5 μm error in the tests with microparts of different sizes, which was analyzed in Section 5.4.3. Without that error, all the accuracies would have been in the same scale. In all test sets the angular accuracies are better than 0.5°. More accurate fabrication is needed to identify the limiting factor in accuracy: whether it is the droplet self-alignment process or the fabrication accuracy of the parts.

Chapter 6

Conclusions

This thesis discussed the effects of different process parameters on droplet self-alignment assisted robotic microhandling. At first the miniaturization in the context of microhandling has been discussed. The state-of-the-art of microassembly strategies in two different branches, robotic assembly and self-assembly, have been presented. Additionally, the idea of hybrid handling methods combining characteristics of both branches has been introduced. The theoretical background of capillary force and its applications in microhandling have also been introduced.

In the experimental part of the thesis, a hybrid handling method combining capillary self-assembly and robotic handling was further studied. The main components of the test setup are a robotic microassembly system with a tweezer-type microgripper, which is used for rough positioning, and a non-contact dispenser, which generates the droplets. The basic experimental procedure includes: A droplet is dispensed on the top of a SU-8 micropart, a robotic system brings another SU-8 part onto the droplet using a microgripper, and capillary forces align the top SU-8 micropart after the part is released from the microgripper.

The concept of the method had already been previously proven. In this thesis the objective was to better understand the effects of process parameters and to see if the dispensing position had any effect on the assembly result. One aspect to observe is the difference from previous results – in previous tests

the dispensing position had been in the middle of the bottom part, while the droplet was dispensed to the center of the releasing position of the top part in the work of this thesis.

The effects of four different parameters, x-bias, y-bias, releasing height and amount of water were systematically studied through several sets of tests. Both 300 µm × 300 µm × 70 µm parts and 100 µm × 100 µm × 70 µm parts were assembled, as well as the assembly of parts of different sizes (a 300 µm × 300 µm × 70 µm part on the top of a 300 µm × 600 µm × 70 µm part) was studied. After the experiments, the accuracy of the assembly was examined using a scanning electron microscope.

The critical part in final alignment of the microparts – the forming of the meniscus – is affected by all parameters. Insufficient amount of water leads to dry contacts between the parts and difficulties in meniscus formation. The size of the parts also affects the amount of water needed to wet the whole contact area – for smaller parts, the amount of water required is not as large as with larger parts. A meniscus was not formed at all when the top part was released from too high a distance. However, a too low releasing position makes it easier for the water to flow away from the gap between the parts. A coupling between the amount of water and the releasing height has been observed: when there is more water, more space is needed between the parts.

The x- and y-biases affected clearly the success rate – when the droplet lands outside of the bottom part, success is not possible. That is clearly different from the previous result (Sariola et al., 2008b) when the droplet was dispensed at the center of the bottom part regardless of the biases in releasing – when the droplet was always on the top of the bottom part, larger biases led to successful alignments. In the assembly tests with a small part on a large part, some failures cannot directly be explained by the parameters, but by the geometric configuration.

The accuracy of the hybrid method is fully competitive with robotics only methods. Even the most accurate robotic manipulators may have problems with the object adhering to the end effector which deteriorates the final accuracy in positioning. Moreover, the accuracy of the robotic solutions are limited by the sensors, which determines how accurately the target position

can be located. With the hybrid microhandling method studied in this thesis, however, the above-mentioned adhering problem can be avoided and the accuracy requirements on the robotic positioning is low, because the final phase is performed by self-assembly. Assembly accuracies close to the fabrication accuracy of the microparts can be achieved (about 2 μm) and accuracy in fabrication must be ameliorated to reach better accuracies. The angular RMS error was a maximum of 0.5° within the tests.

The experimental study shows that the method is well capable of handling 300 μm × 300 μm and 100 μm × 100 μm microparts, and can even assemble parts of different sizes on the top of another. The parameter values obtained in this thesis can be used as a basis for future scientific study as well as industrial applications. Some parameters such as the properties of the liquid clearly have an effect on the assembly. The precise nature of these effects is left for further studies.

References

S. Abbasi, A. X. Zhou, R. Baskaran, and K. F. Böhringer. Part tilting in capillary-based self-assembly: modeling and correction methods. *IEEE 21st International Conference on Micro Electro Mechanical Systems*, 2008.

A. Albut, Q. Zhou, C. del Corral, and H. N. Koivo. Development of a flexible force-controlled piezo-bimorph microgripping system. *Proceedings of 2nd VDE World Microtechnologies Congress, MICRO.tec*, pages 507–512, Oct. 2003.

A. Avital and E. Zussman. Fluidic assembly of optical components. *IEEE transactions on advanced packaging*, 29(4):719–724, 2006.

C. Bark, T. Binnenbose, G. Vogele, T. Weisener, and M. Widmann. Gripping with low viscosity fluids. *Proceedings of the Eleventh Annual International Workshop on Micro Electro Mechanical Systems*, 1998.

R. Baskaran, J. H. Hoo, B. Cheng, and K. F. Böhringer. Catalyst enhanced micro scale batch assembly. *International Conference on Micro Electro Mechanical Systems*, 2008.

K. F Böhringer. Surface modification and modulation in microstructures: controlling protein adsorption, monolayer desorption and micro-self-assembly. *Journal of micromechanics and microengineering*, 13, 2003.

K. F. Böhringer, U. Srinivasan, and R. T. Howe. Modeling of capillary forces and binding sites for fluidic self-assembly. *The 14th IEEE International Conference on Micro Electro Mechanical Systems*, pages 369–374, 2001.

M. Boncheva and G. M. Whitesides. Making things by self-assembly. *MRS Bulletin*, Oct. 2005.

E. J. Bos, J. E. Bullema, P. H. J. Schellekens F. L. M. Delbressine, and A. Dietzel. A lightweight suction gripper for micro assembly. *Precision Engineering*, 32:100–105, 2008.

N. Bowden, A. Terfort, J. Carbeck, and G. M. Whitesides. Self-assembly of mesoscale objects into ordered two-dimensional arrays. *Science*, 276(5310): 233–235, 1997.

K. Brakke. The surface evolver. *Experimental Mathematics*, 1(2):141–165, 1992.

L. Brammer. Developments in inorganic crystal engineering. *Chem. Soc. Rev.*, 33:476–489, 2004.

B. Chang, Q. Zhou, J. Wang, and H. N. Koivo. Capillary forces modeling in micro/nano interactions. *Proceedings of the ASME 2007 International Conference on Integration and Commercialization of Micro- and Nanosystems*, pages 1005–1016, 2007.

N. Chronis and L. P. Lee. Electrothermally activated SU-8 microgripper for single cell manipulation in solution. *Journal of microelectromechanical systems*, 14(4), 2005.

P. B. Chu and S. J. Pister. Analysis of closed-loop control of parallel-plate electrostatic microgrippers. *1994 IEEE International Conference on Robotics and Automation*, 1:820–825, 1994.

M. B. Cohn. Method and apparatus for the assembly of microfabricated devices, US patent no. 5,355,577, Oct 1994.

M. B. Cohn, C.-J. Kim, and A. P. Pisano. Self-assembling electrical networks: An application of micromachining technology. *Proc. 6th Int. Conf. Solid-State Sensors and Actuators*, pages 490–493, 1991.

M. B. Cohn, K. F. Böhringer, J. M. Noworolski, A. S., C. G. Keller, K. A. Goldberg, and R. T. Howe. Microassembly technologies for MEMS. *Proc. SPIE*, 3513(2), 1998.

N. Dechev, W. L. Cleghorn, and J. K. Mills. Microassembly of 3-D microstructures using a compliant, passive microgripper. *Journal of Microelectromechanical Systems*, 13(2):176–189, 2004.

C. del Corral, Q. Zhou, A. Albut, B. Chang, S. Franssila, S. Tuomikoski, and H. N. Koivo. Droplet based self-assembly of SU-8 microparts. *Proceedings MICRO.tec - 2nd VDE World Microtechnologies Congress*, pages 293–298, 2003.

N. D. Denkov, O. D. Velev, P. A. Kralchevsky, I. B. Ivanov, H. Yoshimura, and K. Nagayama. Mechanism of formation of two-dimensional crystals from latex particles on substrates. *Langmuir*, 8:3183–3190, 1992.

H. Du, C. Su, M. K. Lim, and W. L. Jin. A micromachined thermally-driven gripper: a numerical and experimental study. *Smart materials & structures*, 8(5):616–622, 1999.

J. Fang and K. F. Böhringer. Wafer-level packaging based on uniquely orienting self-assembly (the DUO-SPASS processes). *Journal of Microelectromechanical Systems*, 15(3), 2006.

J. Fang, S. Liang, K. Wang, X. Xiong, and K. F. Böhringer. Self-assembly of flat micro components by capillary forces and shape recognition. *Conference on Foundations of Nanoscience: Selfassembled Architectures and Devices*, 2005.

G. Fantoni and M. Porta. A critical review of releasing stategies in microparts handling. *Micro-Assembly Technologies and Applications: proceedings of the Fourth International Precision Assembly Seminar*, 2008.

R. S. Fearing. Survey of sticking effects for micro parts handling. *IEEE/RSJ Conf. on Intell. Robots and Systems*, 2:212–217, 1995.

J. T. Feddema, P. Xavier, and R. Brown. Micro-assembly planning with van der waals force. *Proceedings of the 1999 IEEE International Symposium on Assembly and Task Planning*, 1999.

S. Franssila. *Introduction to microfabrication*. Wiley, 2004.

T. Fukuda and T. Tanaka. Micro electrostatic actuator with three degrees of freedom. In *An Investigation of Micro Electro Mechanical Systems, 1990. Proceedings*, pages 153–158, Feb. 1990.

D. H. Gracias, J. Tien, T. L. Breen, C. Hsu, and G. M. Whitesides. Forming electrical networks in three dimensions by self-assembly. *Science*, 289: 1170–1172, 2000.

P. W. Green, R. R. A. Syms, and E. M. Yeatman. Demonstration of three-dimensional microstructure self-assembly. *Journal of microelectromechanical systems*, 4(4):170–176, 1995.

A. Greiner, J. Lienemann, J. G. Korvink, X. Xiong, Y. Hanein, and K. F. Böhringer. Capillary forces in micro-fluidic self-assembly. *Technical Proceedings of the International Conference on Modeling and Simulation of Microsystems*, 1:198–201, 2002.

H. Grutzeck. Investigations of the capillary effect for gripping silicon chips. *Microsystem Technologies*, 11:194–203, 2005.

H. Grutzeck and L. Kiesewetter. Downscaling of grippers for micro assembly. *Microsystem Technologies*, 8(1):27–31, 2002.

B. A. Grzybowski, N. Bowden, F. Arias, H. Yang, and G. M. Whitesides. Modeling of menisci and capillary forces from the millimeter to the micrometer size range. *Journal of Physical Chemistry B*, 105:404–412, 2001.

Y. Haddab, N. Chaillet, and A. Bourjault. A microgripper using smart piezoelectric actuators. *Proceedings of the 2000 IEEE/RSJ International Conference on Intelligent Robots and Systems*, 1:659–664, 2000.

I. W. Hunter, S. Lafontaine, P. M. F. Nielsen, P. J. Hunter, and J. M. Hollerbach. Manipulation and dynamic mechanical testing of microscopic objects using a tele-micro-robot system. In *Proceedings of 1989 IEEE International Conference on Robotics and Automation*, volume 3, pages 1553–1558, 1989.

J. N. Israelachvili. *Intermolecular and surface forces.* Academic Press, 1985.

IUPAC. *Compendium of Chemical Terminology.* ed. A. D. McNaught and A.Wilkinson, Blackwell Scientific Publications, Oxford, 1997.

M. Jääskeläinen, V. Sariola, and Q. Zhou. Environmental effects on droplet self-alignment assisted hybrid microassembly. *Proceedings of 2009 IEEE International Symposium on Assembly and Manufacturing*, pages 177–182, 2009.

A. Kochan. European project develops "ice" gripper for micro-sized components. *Assembly automation*, 17(2):114–115, 1997.

M. Kohl, E. Just, W. Pfleging, and S. Miyazaki. SMA microgripper with integrated antagonism. *Sensors and Actuators A: Physical*, 83(1-3):208–213, 2000.

P. Lambert. *Capillary forces in microassembly.* Springer, 2007.

P. Lambert and A. Delchambre. Design rules for a capillary gripper in microassembly. *The 6th IEEE International Symposium on Assembly and Task Planning: From Nano to Macro Assembly and Manufacturing*, pages 67–73, 2005.

P. Lambert and S. Régnier. Surface and contact forces models within the framework of microassembly. *Journal of micromechatronics*, 3(2), 2006.

A. P. Lee, D. R. Ciarlo, P. A. Krulevitch, S. Lehew, J. Trevino, and M. A. Northrup. A practical microgripper by fine alignment, eutectic bonding and SMA actuation. *Sensors and Actuators A: Physical*, 54(1-3):755–759, 1996.

C. Lin, F. Tseng, and C.-C. Chieng. Uni-direction orienting and size effect automatic alignment using capillary based in fluidic self-assembly process. *Proceedings of 2nd International Conference on Innovative Computing, Information and Control, ICICIC*, 2007.

C. Lin, F. Tseng, and C.-C. Chieng. Orientation-specific fluidic self-assembly process based on a capillary effect. *Journal of micromechanics and microengineering*, 19, 2009.

J. Liu, Y.-X. Zhou, and T.-H. Yu. Freeze tweezer to manipulate mini/micro objects. *Journal of Micromechanics and Microengineering*, 14:269–276, 2004.

B. López-Walle, M. Gauthier, and N. Chaillet. Principle of a submerged freeze gripper for microassembly. *IEEE Transactions on Robotics,*, 24(4): 897–902, 2008.

M. Mastrangeli, S. Abbasi, C. Varel, C. Van Hoof, J.-P. Celis, and K. F. Böhringer. Self-assembly from milli- to nanoscales: methods and applications. *Journal of micromechanics and microengineering*, 19, 2009.

O. Millet, P. Bernardoni, S. Régnier, P. Bidaud, E. Tsitsiris, D. Collard, and L. Buchaillot. Electrostatic actuated micro gripper using an amplification mechanism. *Sensors and Actuators A: Physical*, 114(2-3):371–378, 2004.

C. J. Morris, S. A. Stauth, and B. A. Parviz. Self-assembly for microscale and nanoscale packaging: Steps toward self-packaging. *IEEE Transactions on Advanced Packaging*, 28(4):600–611, 2005.

K. J. Obata, T. Motokado, S. Saito, and K. Takahashi. A scheme for micro-manipulation based on capillary force. *Journal of Fluid Mechanics*, 498: 113–121, 2004.

E. Saeedi, S. Abbasi, K. F. Böhringer, and B. A. Parviz. Molten-alloy driven self-assembly for nano and micro scale system integration. *Fluid Dynamics and Materials Processing*, 2(4):221–245, 2006.

P. Salomon. Micro sensors – world wide markets and economic impact. *Eurosensors Göteborg*, 2006.

V. Sariola, Q. Zhou, and H. N. Koivo. Hybrid microhandling: a unified view of robotic handling and self-assembly. *Journal of Micro - Nano Mechatronics*, 4(1-2):5–16, Nov. 2008a.

V. Sariola, Q. Zhou, R. Laaß, and H. N. Koivo. Experimental study on droplet based hybrid microhandling using high speed camera. *IEEE/RSJ International Conference on Intelligent Robots and Systems, IROS*, pages 919–924, 2008b.

K. Sato, K. Ito, S. Hata, and A. Shimokohbe. Self-alignment of microparts using liquid surface tension – behavior of micropart and alignment characteristics. *Precision Engineering*, 27(1):42–50, 2003.

M. A. Schmidt. Wafer-to-wafer bonding for microstructure formation. *Proceedings of the IEEE*, 86(8), 1998.

I. Shimoyama. Scaling in microrobots. *Proceedings of the International Conference on Intelligent Robots and Systems*, 2:208–211, 1995.

U. Srinivasan, D. Liepmann, and R. T. Howe. Microstructure to substrate self-assembly using capillary forces. *Journal of microelectromechanical systems*, 10(1):17–24, 2001.

S. A. Stauth and B. A. Parviz. Self-assembled single-crystal silicon circuits on plastic. *Proceedings of the National Academy of Sciences*, 103(38):13922–13927, 2006.

A. Terfort, N. Bowden, and G. M. Whitesides. Three-dimensional self-assembly of millimetre-scale components. *Nature*, 386:162–164, 1997.

M. Tichem, D. Lang, and B. Karpuschewski. A classification sceme for quantitative analysis of micro-grip principles. *Assembly automation*, 24 (1):88–93, 2004.

A. Torkkeli. *Droplet microfluidics on a planar surface*. VTT Technical Research Centre of Finland, 2002.

W. S. N. Trimmer. Microrobots and micromechanical systems. *Sensors and actuators*, 19:267–287, 1989.

C. G. Tsai, C. M. Hsieh, and J. A. Yeh. Self-alignment of microchips using surface tension and solid edge. *Sensors and Actuators A: Physical*, 139 (1-2):343–349, 2007.

T. Tsuchiya, O. Tabata, J. Sakata, and Y. Taga. Specimen size effect on tensile strength of surface-micromachined polycrystalline silicon thin films. *Journal Of Microelectromechanical Systems*, 7(1):106–113, 1998.

S. Tuomikoski, C. del Corral, Q. Zhou, and S. Franssila. SU-8 as a mechanical material: gripper tips and microparts for a microassembly robot. *Proceedings of the 14th Micromechanic Workshop, MME3*, 2003.

V. Vandaele, P. Lambert, and A. Delchambre. Non-contact handling in microassembly: Acoustical levitation. *Precision Engineering*, 29:491–505, 2005.

A. Vasudev and J. Zhe. A capillary microgripper based on electrowetting. *Applied physics letters*, 93, 2008.

C. Waltham, S. Bendall, and A. Kotlicki. Bernoulli levitation. *American Journal of Physics*, 71(2):176–179, Feb. 2003.

M. Wautelet. Scaling laws in the macro-, micro- and nanoworlds. *European Journal of Physics*, 22:601–611, 2001.

G. M. Whitesides and B. Grzybowski. Self-assembly at all scales. *Science*, 295, Mar. 2002.

X. Xiong, Y. Hanein, W. Wang, D. T. Schwartz, and K. F. Böhringer. Multi-batch micro-self-assembly via controlled capillary forces. *Proceedings of International Conference on Intelligent Robots and Systems*, pages 1335–1342, 2001.

H.-J. J. Yeh and J. S. Smith. Fluidic self-assembly for the integration of GaAs light-emitting diodes on Si substrates. *IEEE Photonics Technology Letters*, 6(6):706–708, 1994.

Q. Zhou and V. Sariola. *Robotic microassembly*, chapter Unified view of robotic microhandling and self-assembly. ed. M. Gauthier and S. Régnier, Wiley-Interscience, 2009.

Q. Zhou, A. Aurelian, B. Chang, C. del Corral, and H. N. Koivo. Microassembly system with controlled environment. *Journal of Micromechatronics*, 2, 2004.

Q. Zhou, B. Chang, and H. N. Koivo. Temperature and humidity effects on micro/nano handling. *Materials Science Forum*, 532-533:681–684, 2006a.

Q. Zhou, P. Korhonen, J. Laitinen, and S. Sjövall. Automatic dextrous microhandling based on a 6-DOF microgripper. *Journal of Micromechatronics*, 3(3-4):359–387, 2006b.